UNIVERSIDADE
BEIRA INTERIOR

Development of multifunctional IR780 based nanomaterials for cancer therapy

Miguel Marques Leitão

Dissertação para obtenção do Grau de Mestre em
Ciências Biomédicas
(2º ciclo de estudos)

Orientador: Doutor Duarte Miguel de Melo Diogo
Co-orientador: Prof. Doutor Ilídio Joaquim Sobreira Correia
Co-orientador: Mestre Cátia Gomes Alves

setembro de 2020

“Science never solves a problem without creating ten more”

- George Bernard Shaw

Dedication

Dedico este trabalho à minha família, à Ariana, ao senhor Quirino e a todos os que me deram apoio ao longo de todo o meu percurso académico.

Acknowledgments

Em primeiro lugar quero agradecer ao Professor Doutor Ilídio Correia, por me ter dado a oportunidade de realizar a tese no seu grupo de investigação. Quero agradecer-lhe pela sua co-orientação, experiência e conselhos que foram essenciais para o desenvolvimento do meu trabalho. Quero ainda agradecer, por partilhar outro tipo de ensinamentos que me tornaram uma pessoa mais atenta no mundo que nos rodeia.

Ao meu orientador Doutor Duarte Diogo, quero agradecer por todo apoio, paciência e dedicação que me deu, que permitiu ultrapassar as longas barreiras impostas por este trabalho e me tornar numa pessoa cada vez melhor.

À minha co-orientadora Mestre Cátia Alves, agradeço o esforço, paciência e por todos os ensinamentos que me deu, tornado esta etapa mais simples.

Agradeço também a todos os elementos do grupo de investigação pela ajuda e disponibilidade que mostraram ao longo ano.

Aos meus camaradas de serviço, Ivo e Natanael, um profundo agradecimento por me ajudarem sempre que precisei sem nunca hesitar e por tornarem este ano mais curto. Em especial ao Ivo, que apesar das circunstâncias, esteve sempre disposto a ajudar-me independentemente da situação.

Quero ainda agradecer à minha família por todo o apoio que me deu ao longo de todos estes anos, sem eles isto não seria possível.

Por fim quero agradecer à Ariana por tudo, pois sem ela jamais eu teria completado estes anos da minha vida, sendo o meu pilar, a força que me apoiou em todos os momentos. Muito, muito obrigado.

Resumo

O cancro da mama é o tipo de cancro que mais afeta as mulheres. Este cenário deve-se às limitações das terapias utilizadas em meio clínico (quimioterapia e radioterapia), as quais apresentam uma baixa eficácia e efeitos secundários associados. Desta forma, existe uma necessidade premente de desenvolver estratégias inovadoras para o tratamento deste tipo de cancro.

Na atualidade, diferentes grupos de investigação estão focados no desenvolvimento de nanomateriais para aplicação na terapia fototérmica do cancro. Este tipo de abordagem terapêutica tem por base a acumulação dos nanomateriais na região tumoral e a sua posterior irradiação com luz com um comprimento de onda na zona do infravermelho próximo (em inglês: *Near Infrared* (NIR)). Os nanomateriais acumulados no tumor absorvem esta radiação e convertem-na em calor que causa danos nas células cancerígenas.

Entre os diferentes nanomateriais desenvolvidos até ao momento, o óxido de grafeno (em inglês: *Graphene Oxide* (GO)) apresenta-se como um candidato bastante promissor para aplicação na terapia fototérmica do cancro devido à sua capacidade de absorção no NIR e de encapsulamento de biomoléculas. Contudo, o GO apresenta uma baixa estabilidade coloidal, *i.e.,* precipita facilmente quando em contacto com fluídos biológicos. Para além disto, este nanomaterial possui uma baixa capacidade fototérmica, sendo preciso recorrer à administração de elevadas doses ou ao uso de radiação NIR intensa de forma a alcançar um efeito terapêutico adequado.

No trabalho de investigação desenvolvido durante o meu segundo ano de mestrado, o GO foi revestido com um polímero anfifílico contendo segmentos de metacrilato de sulfobetaína (SBMA) de forma a aumentar a sua estabilidade coloidal. Posteriormente, o IR780 foi incorporado neste nanomaterial funcionalizado, com o objetivo de melhorar a sua capacidade fototérmica.

Os resultados obtidos no presente estudo demonstraram que o GO funcionalizado com SBMA apresenta uma carga de superfície neutra e que é citocompatível. Para além disso, o GO funcionalizado com SBMA manteve a sua distribuição de tamanhos praticamente inalterada, pelo menos durante 48 h, quando em contacto com meio com relevância biológica, possuindo assim uma elevada estabilidade coloidal. Em contraste, os nanomateriais de GO não funcionalizados precipitaram rapidamente em meio de cultura

celular. Ao encapsular o IR780 no GO funcionalizado com SBMA, a sua absorção no NIR (a 808 nm) aumentou em cerca de 2,7 vezes, o que lhe permitiu gerar um aumento de temperatura que foi 1,2 vezes maior. Nos estudos *in vitro*, a conjugação da luz NIR com o GO funcionalizado com SBMA apenas reduziu a viabilidade das células do cancro da mama para 73 %. Em contraste, a combinação da luz NIR com GO funcionalizado com SBMA contendo o IR780, induziu uma redução da viabilidade das células cancerígenas para 20 %. Estes resultados confirmam o potencial deste nanomaterial para aplicação na terapia fototérmica do cancro da mama.

Palavras-chave

Cancro;IR780;óxido de grafeno;revestimentos zwiteriónicos;terapia fototérmica.

Resumo alargado

Atualmente, o cancro é uma das doenças que mais afeta a população mundial. Em particular, o cancro da mama é o tipo de cancro que mais afeta as mulheres. Este cenário deve-se às limitações das terapias utilizadas em meio clínico (quimioterapia e radioterapia), as quais apresentam uma baixa eficácia e efeitos secundários associados. Desta forma, existe uma necessidade premente de desenvolver estratégias inovadoras para o tratamento deste tipo de cancro.

De forma a colmatar estas limitações, atualmente diferentes grupos de investigação estão focados no desenvolvimento de nanomateriais para aplicação na terapia fototérmica do cancro. Este tipo de abordagem terapêutica tem por base a acumulação dos nanomateriais na região tumoral e a sua posterior irradiação com luz com um comprimento de onda na zona do infravermelho próximo (em inglês: *Near Infrared* (NIR); 750-1000 nm). Neste tipo de aplicação, a utilização de luz NIR é fundamental devido à sua baixa interação com os componentes biológicos (tais como água, proteínas, melanina) e à sua elevada capacidade de penetração nos tecidos. Os nanomateriais acumulados no tumor absorvem esta radiação, e convertem-na em calor que causa danos nas células cancerígenas.

Assim, os nanomateriais utilizados na terapia fototérmica do cancro devem ter capacidade para absorver na região do NIR. Entre os diferentes nanomateriais desenvolvidos até ao momento, o óxido de grafeno (em inglês: *Graphene Oxide* (GO)) apresenta-se como um candidato bastante promissor para aplicação na terapia fototérmica do cancro devido à sua capacidade de absorção no NIR e de encapsulamento de biomoléculas. Contudo, o GO apresenta uma baixa estabilidade coloidal*, i.e.,* precipita facilmente quando em contacto com fluídos biológicos. Para além disto, este nanomaterial possui uma baixa capacidade fototérmica, sendo preciso recorrer à administração de elevadas doses ou ao uso de radiação NIR intensa de forma a alcançar um efeito terapêutico adequado.

No trabalho de investigação desenvolvido durante o meu segundo ano de mestrado, o GO foi revestido com um polímero anfifílico contendo segmentos de metacrilato de sulfobetaína (SBMA). Posteriormente o IR780 foi incorporado neste nanomaterial funcionalizado, de forma a explorar o mesmo na terapia fototérmica do cancro da mama. O GO foi funcionalizado com um polímero contendo segmentos de SBMA, uma vez que estes segmentos já foram descritos como sendo capazes de aumentar a estabilidade

coloidal e o tempo de circulação de nanomateriais, favorecendo a acumulação destes no tumor. Por sua vez, o IR780 foi incorporado no GO por ser um agente responsivo à luz NIR com potencial para melhorar a capacidade fototérmica deste nanomaterial.

Para obter o polímero anfifílico contendo o SBMA, esta molécula foi conjugada com poli(etilenoimina) (PEI), sendo o polímero obtido posteriormente ligado quimicamente ao poli(anidrido maleico-*alt*-1-octadeceno) (PMAO) hidrolisado. O polímero resultante desta síntese (SBMA-PEI-PMAO (SPP)), foi posteriormente utilizado para revestir o GO através de um processo de sonicação, obtendo-se o SPP/GO. Através do mesmo processo, procedeu-se ao encapsulamento do IR780 no SPP/GO (IR780-SPP/GO).

Os resultados obtidos no presente estudo demonstraram que o SPP/GO e o IR780-SPP/GO apresentam uma carga de superfície neutra e uma distribuição de tamanhos que se mantém praticamente inalterada, pelo menos durante 48 h, quando em contacto com meio com relevância biológica, demonstrando assim uma elevada estabilidade coloidal. Em contraste, os nanomateriais de GO não funcionalizados com SBMA (GO revestido com PEI-PMAO e GO revestido com PEI-PMAO contendo IR780) precipitaram rapidamente em meio de cultura celular. Ao encapsular o IR780 no SPP/GO, a sua absorção no NIR (a 808 nm) aumentou em cerca de 2,7 vezes. Assim, quando irradiado com luz NIR, o IR780-SPP/GO conseguiu gerar um aumento de temperatura que foi 1,2 vezes superior ao que foi produzido pelo SPP/GO. Nos estudos *in vitro*, a conjugação da luz NIR com o SPP/GO apenas reduziu a viabilidade das células do cancro da mama para 73 %. Em contraste, a combinação da luz NIR com IR780-SPP/GO levou a uma redução da viabilidade das células cancerígenas para 20 %. Estes resultados confirmam o potencial do IR780-SPP/GO para aplicação na terapia fototérmica do cancro da mama.

Abstract

Breast cancer is a common cause of death among women. This scenario is in part explained by the limitations presented by the treatments currently used in the clinic (*e.g.* radiotherapy, chemotherapy), which display a low therapeutic efficacy and induce adverse side effects. In this way, it is necessary to develop innovative strategies that propel the breast cancer therapy efficacy.

Among the different therapeutic strategies under investigation, cancer photothermal therapy mediated by nanomaterials has been showing promising results. This type of therapy takes advantage from the nanomaterials' physico-chemical properties, that enable their tumor accumulation. Subsequently, the tumor zone is irradiated with Near Infrared (NIR; 750-1000 nm) light and the tumor-homed nanomaterials absorb this energy, releasing it as heat that causes damage to cancer cells.

From the plethora of nanomaterials with potential to be applied in cancer photothermal therapy, Graphene Oxide (GO) is a promising candidate due to its NIR absorption and loading capacity. However, as-synthesized GO lacks colloidal stability, *i.e.,* it precipitates when in contact with biological fluids. On the other hand, GO displays a modest photothermal capacity, requiring the use of high doses or intense radiation to achieve the desired therapeutic effect.

In the work developed during my MSc, GO was functionalized with an amphiphilic polymer containing [2-(methacryloyloxy)ethyl]dimethyl-(3-sulfopropyl)ammonium hydroxide (SBMA) brushes and was loaded with IR780 (a NIR photoabsorber), for the first time, to improve its colloidal stability and phototherapeutic capacity, respectively. The obtained results revealed that the SBMA-functionalized GO displays a suitable size distribution, neutral surface charge and an appropriate cytocompatibility. Furthermore, the SBMA-functionalized GO exhibited an improved colloidal stability in biological relevant media (at least up to 48 h), while GO without SBMA functionalization promptly precipitated in the same conditions. By loading IR780 into the SBMA-functionalized GO, its NIR absorption increased by 2.7-fold (at 808 nm), leading to a 1.2-times higher photothermal heating. In *in vitro* cell studies, the conjugation of NIR irradiation with SBMA-functionalized GO could reduce breast cancer cells' viability to 73 %. In stark contrast, by combining IR780 loaded SBMA-functionalized GO and NIR radiation, the cancer cells' viability decreased to 20 %. Overall, the IR780 loaded SBMA-functionalized

GO nanomaterials have promising properties for application in breast cancer phototherapy.

Keywords

Cancer, graphene oxide, IR780, photothermal therapy, zwitterionic coatings.

List of Publications

Articles published in international peer reviewed journals:

Leitão, M. M., de Melo-Diogo, D., Alves, C. G., Lima-Sousa, R., Correia, I. J., 2020. *Prototypic Heptamethine Cyanine Incorporating Nanomaterials for Cancer Phototheragnostic*. Advanced Healthcare Materials 9, 1901665 (DOI: 10.1002/adhm.201901665).

Articles submitted for publication in international peer reviewed journals:

Leitão, M. M., Alves, C. G., de Melo-Diogo, D., Lima-Sousa, R., Correia, I. J.; *Sulfobetaine methacrylate-functionalized graphene oxide-IR780 nanohybrids aimed for improved breast cancer phototherapy*. Under review.

Index

Figure Index

List of Abbreviations

ABC	Accelerated Blood Clearance
ANOVA	Analysis of Variance
CLSM	Confocal Laser Scanning Microscopy
DLS	Dynamic Light Scattering
DMEM-F12	Dulbecco's Modified Eagle's Medium-F12
DMSO	Dimethyl Sulfoxide
EDC	1-Ethyl-3-(3-dimethylaminopropyl)carbodiimide
EPR	Enhanced Permeability and Retention
FBS	Fetal Bovine Serum
FTIR	Fourier Transform Infrared Spectroscopy
GO	Graphene Oxide
IR780-PP/GO	IR780 loaded PEI-PMAO functionalized GO
IR780-SPP/GO	IR780 loaded SBMA-PEI-PMAO functionalized GO
MCF-7	Michigan Cancer Foundation-7
MTS	3-(4,5-dimethylthiazol-2-yl)-5-(3-carboxymethoxyphenyl)-2-(4-sulfophenyl)-2H-tetrazolium
NHDF	Normal Human Dermal Fibroblasts
NHS	*N*-Hydroxysuccinimide
NIR	Near Infrared
ns	Non-significant
PEG	Poly(ethylene glycol)
PEI	Poly(ethyleneimine)
PI	Propidium Iodide
PMAO	Poly(maleic anhydride-*alt*-1-octadecene)
PP	PEI-PMAO
PP/GO	PEI-PMAO functionalized GO
PTT	Photothermal Therapy
SBMA	[2-(methacryloyloxy)ethyl]dimethyl-(3-sulfopropyl)ammonium hydroxide
S.D.	Standard Deviation
SP	SBMA-PEI
SPP	SBMA-PEI-PMAO
SPP/GO	SBMA-PEI-PMAO functionalized GO
TEM	Transmission Electron Microscopy

Chapter 1

Introduction

1. Introduction

1.1. Cancer development, hallmarks, and treatments

1.1.1. Cancer

Cancer is one of the most prevalent diseases, being the second leading cause of death worldwide [1]. According to the American Cancer Society, ≈ 1.8 million new cases of cancer are predicted for 2020, as well as about 0.6 million of cancer-related deaths, just in the United States of America [2]. Furthermore, one third of the of deaths caused by cancer were related to smoking, alcohol, obesity, lack of physical activity and eating habits [1].

Cancer is characterized by an uncontrolled growth of cells in response to genetic/epigenetic alterations [3, 4]. During the carcinogenesis, cells adopt specific traits that were designated by Hanahan and co-workers as cancer hallmarks (Figure 1) [5]. These hallmarks include the ability of cancer cells to i) resist to cell death, ii) induce angiogenesis, iii) achieve replicative immortality, iv) activate invasion and metastasis, v) evade growth suppressors, vi) sustain proliferative signalling, vii) modify or reprogram cellular metabolism, and viii) evade immunological destruction. Furthermore, there are two characteristics that facilitate the acquisition of these hallmarks: genome instability and mutation, as well as tumor-promoting inflammation (Figure 1) [3, 5].

In this way, cancer cells arise from the proliferation of mutated cells, where proliferation is sustained by a cascade of growth factors, which the cancer cells produce themselves (autocrine signalling) or by the signalling they induce in neighbouring phenotypically normal cells (paracrine signalling) (Figure 2). The cancer cells' proliferative capacity can also be enabled by changes that occur in the receptors of the signalling molecules [3, 5].

In addition, cancer cells present a dysregulated cell cycle and are capable of suppressing apoptosis through the down regulation of tumor suppressors (such as the P53 protein). The cancer cells also have the ability to decrease the expression of pro-apoptotic proteins (*e.g.* Bax, Bim, Puma) and to increase the expression of anti-apoptotic factors (*e.g.* Bcl-2, Bcl-xL) or survival signals (*e.g.* Igf1/Igf2) [5]. Furthermore, cancer cells present unlimited replicability since they are able to maintain the length of their telomeres by overexpressing telomerase, giving them protection against degradation and/or end-to-end fusion [3, 5, 6].

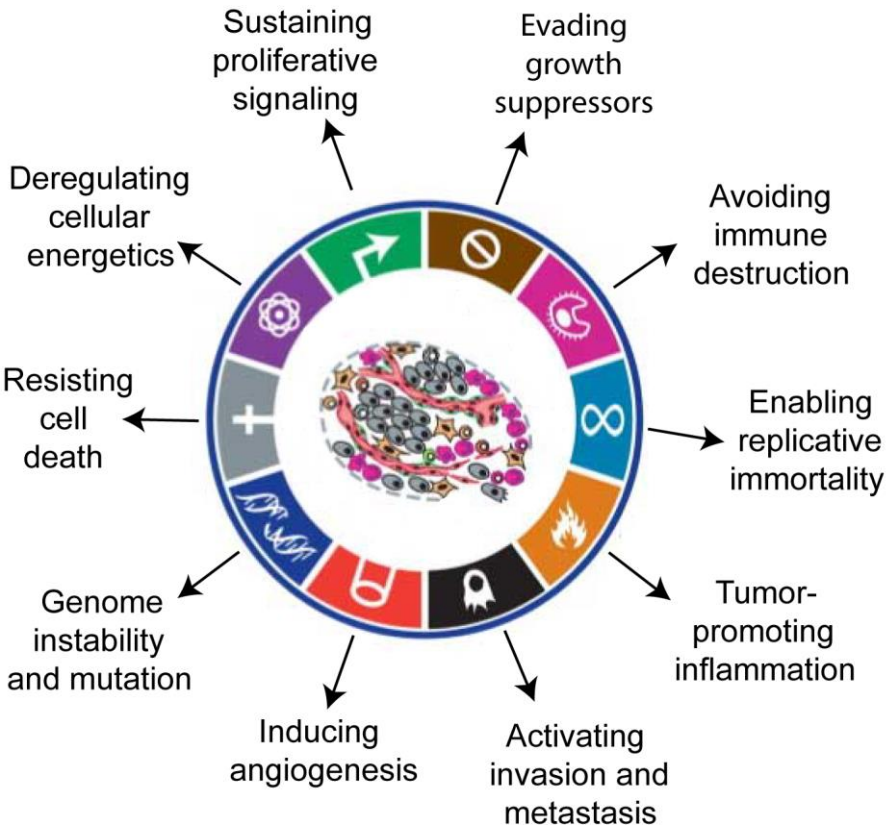

Figure 1: The cancer hallmarks described by Hanahan and Weinberg and the two characteristics that facilitate the acquisition of these hallmarks (Adapted from [5]).

Over time, the tumor reaches a larger size, requiring more nutrients/oxygen, waste elimination, among others. To satisfy these demands, cancer cells stimulate angiogenesis (*e.g.* by secreting VEGF), leading to the formation of a new vasculature that improves the blood supplies to the tumor (Figure 2). Finally, cancer cells acquire the ability to extravasate to other tissues through the newly formed vasculature giving rise to metastases. This process also occurs due to alterations on the expression of cell-cell adhesion molecules (*e.g.* E-cadherin), upregulation of molecules associated with cell migration (*e.g.* N-cadherin) or by the degeneration of the extracellular matrix through proteases [3-5].

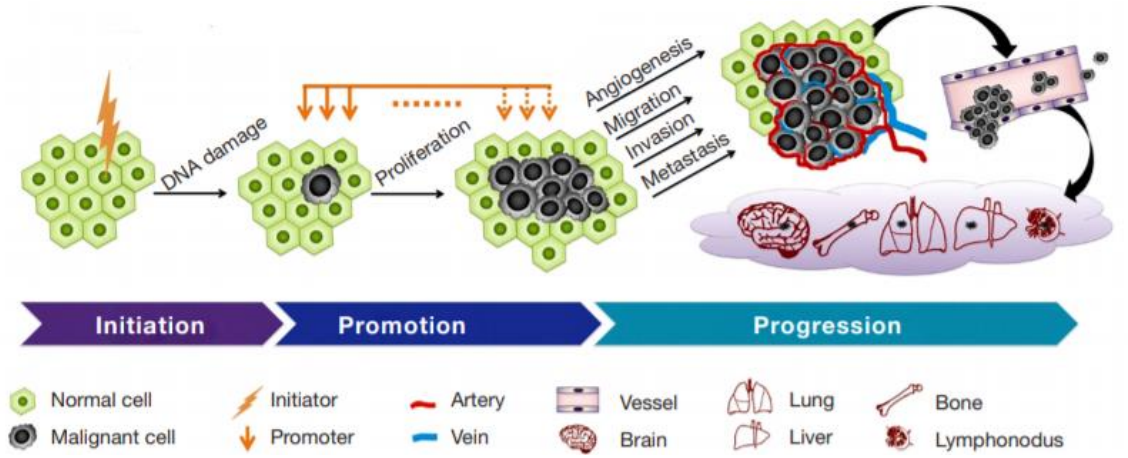

Figure 2: Carcinogenesis process. Different stimuli can cause DNA damage, leading to different mutations in the phenotypically normal cells. If these cells are not eliminated, they will enter in a state of proliferation favoured by different pathways (cascade of growth factors, mutations in signalling receptors, among others). Subsequently, these cells can reach a malignant state with the ability to initiate angiogenesis and invade other tissues (metastatic state) (Adapted from [7]).

Furthermore, cancer cells have several characteristics or mechanisms that make them resistant to certain treatments. For instance, the overexpression of efflux transporters (such as the P-glycoprotein) grants them resistance to chemotherapy [8, 9]. On the other hand, the upregulation of DNA repair machinery endows resistance to radiotherapy [8].

1.1.2. Breast cancer

Breast cancer is the most frequently diagnosed cancer in women, having one of the highest mortality rates [10]. According to the American Cancer Society, 279 100 new cases of breast cancer and 42 690 breast cancer related deaths were predicted to occur in 2020, just in the United States of America [2].

The mammary ducts of healthy breast tissues are composed of luminal epithelial and myoepithelial cells, fixed on the basement membrane, being this later surrounded by stroma constituents (fibroblasts, myofibroblasts, leukocytes and endothelial cells) [11]. The development of breast cancer results from genetic and epigenetic changes in the epithelial cells of breast ducts [11, 12]. These changes lead to a decrease in the number of myoepithelial cells, making them unable to maintain the duct structure [11]. Then, the degradation of the basement membrane and an increase of the stromal cells can occur, leading to a carcinoma *in situ* (Figure 3) [11, 12]. Invasive carcinoma arises when the total loss of the basement membrane and of the myoepithelial cells are attained (Figure 3) [11]. In this state, cancer cells and stromal cells produce a high amount of proteases, which degrade the tumor's extracellular matrix, allowing the cancer cells to invade other tissues where they can form metastases (Figure 3) [11, 12]. In addition,

tumor associated macrophages are also recruited to facilitate the degradation of the extracellular matrix, angiogenesis and tumor invasion [11].

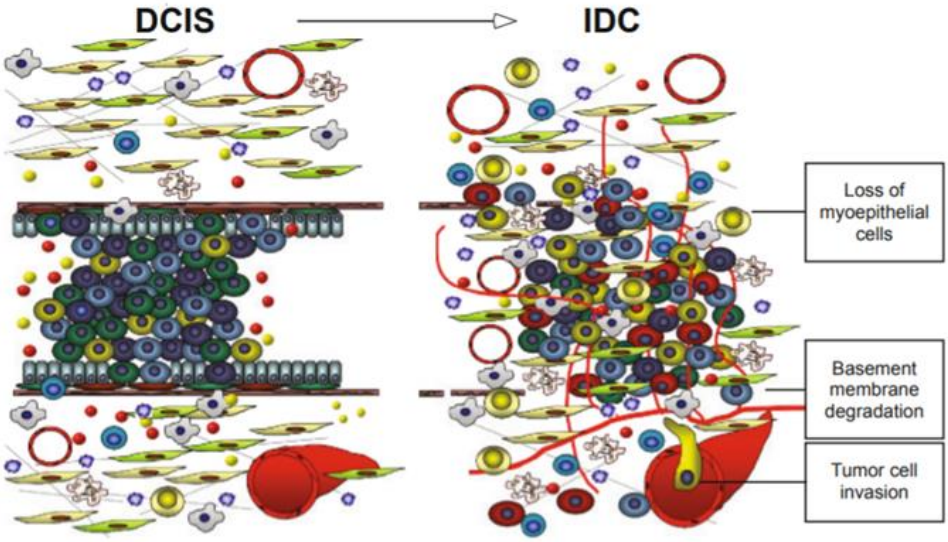

Figure 3: Transition from Ductal Carcinoma *in Situ* (DCIS) to an Invasive Ductal Carcinoma (IDC). IDC is defined by the degradation of the basement membrane, loss of myoepithelial cells and, consequently, the loss of the duct structure. Subsequently, the invasion to neighbouring tissues can occur (Adapted from [11]).

The treatment of breast cancer is dependent on the evolutionary state of the tumor [13, 14]. When the tumor is still localized, surgery is commonly applied to remove the diseased mass. On the other hand, when cancer cells metastasize other tissues, radiotherapy and chemotherapy are the most commonly used approaches [13]. However, these two therapies present a low effectiveness and impose severe side effects to patients (*e.g.* fatigue, pain, cognitive disfunctions), impairing their health and quality of life [13, 15]. Moreover, cancer cells can develop resistance mechanisms to these therapies, further reducing their effectiveness [8, 9]. In this way, new therapeutic modalities with improved effectiveness and safety are needed for treating breast cancer.

1.1.3. Photothermal therapy mediated by nanomaterials

Recently, the development of nanomaterials aimed for cancer Photothermal Therapy (PTT) has been one of the focus of the scientific community [16]. This therapeutic modality employs nanostructures with well-defined physicochemical properties that give them the ability to accumulate preferentially within the tumor zone after intravenous administration. This preferential tumor accumulation occurs due to the Enhanced Permeability and Retention (EPR) effect: i) nanomaterials can accumulate at the tumor tissue by extravasating through the tumor-associated blood vessels, which present fenestra of variable size (200-1200 nm); and ii) nanomaterials remain confined at the

tumor site due to the impaired lymphatic drainage of this zone (Figure 4) [17, 18]. Recently, it was also unveiled that nanomaterials can achieve tumor uptake by extravasating through the dynamic vents (also called eruptions), that dynamically occurs in the tumor vasculature. In this way, nanomaterials should present a high blood circulation time in order to achieve tumor accumulation by taking advantage from the static and dynamic ruptures [19]. After the nanomaterials' accumulation in the tumor zone, the tumor site is externally irradiated with light (Figure 4) [17].

In this regard, the use of Near Infrared (NIR) radiation (750-1000 nm) is of extreme importance since it has high penetration depth and low interaction with biological components (*e.g.* proteins, melanin, water) (Figure 5) [17, 20]. Thereby, it is extremely important to use nanomaterials with a high NIR absorption in cancer PTT [17, 21].

After interacting with the NIR light, nanomaterials absorb its energy, converting it into heat. Depending on the temperature reached, the photoinduced heat can cause reversible (41 °C-45 °C; through impaired metabolic functions, inhibition of DNA repair mechanisms, sensibilization of cells to the action of other therapies) or irreversible (above 50 °C; coagulative necrosis) damage to cancer cells [22, 23].

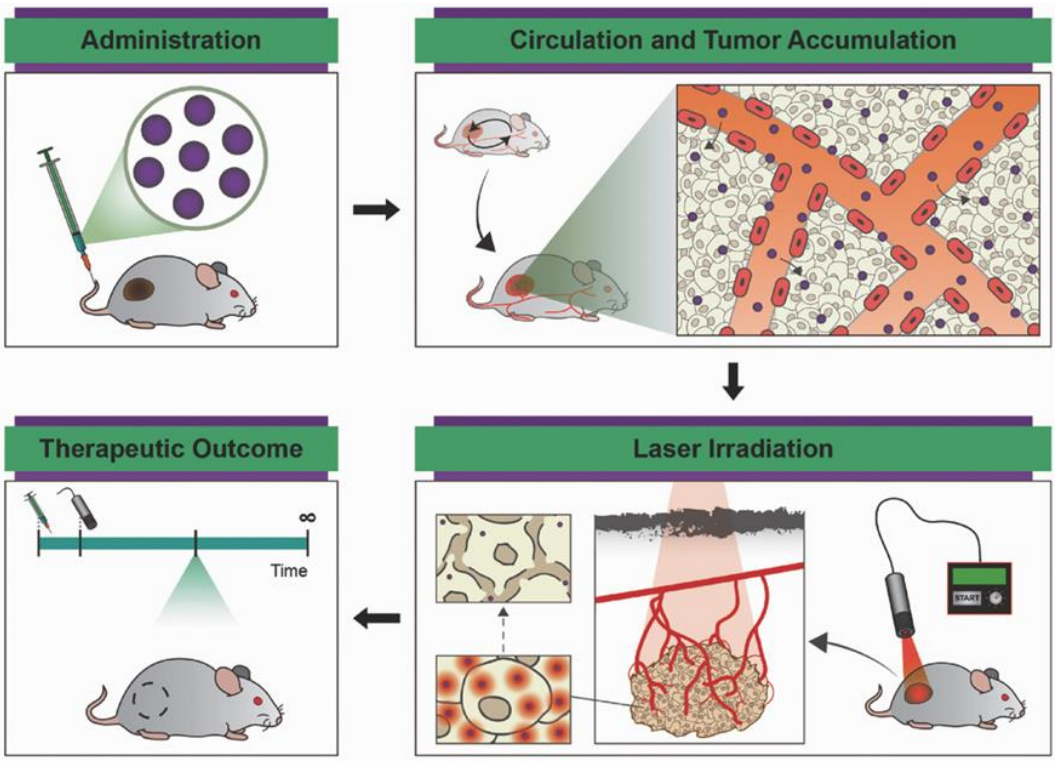

Figure 4: Schematic representation of various events occurring in nanomaterials-based PTT. Initially, nanomaterials are administered intravenously and can accumulate passively in the tumor zone. Then, the tumor area is irradiated with NIR light, and the nanomaterials absorb this energy, converting it into heat. Finally, tumor ablation can be achieved depending on the temperature attained (Adapted from [17]).

Up to now, several types of nanomaterials with photothermal capabilities have been developed [24-26]. In general, inorganic based nanostructures with NIR responsiveness have been the most investigated for cancer PTT due to their excellent photostability. This list includes gold based nanostructures (*e.g.* gold nanorods, gold nanocages), carbon based nanomaterials (*e.g.* carbon nanotubes, Graphene Oxide (GO)), transition metal nanoagents (*e.g.* copper nanoparticles), among others [24, 27-29]. Furthermore, organic based nanoagents such as those formulated with polyaniline, polypyrrole or those incorporating NIR absorbing small molecules (*e.g.* IR780, cypate, IR783) have also demonstrated promising results for cancer PTT [16, 30].

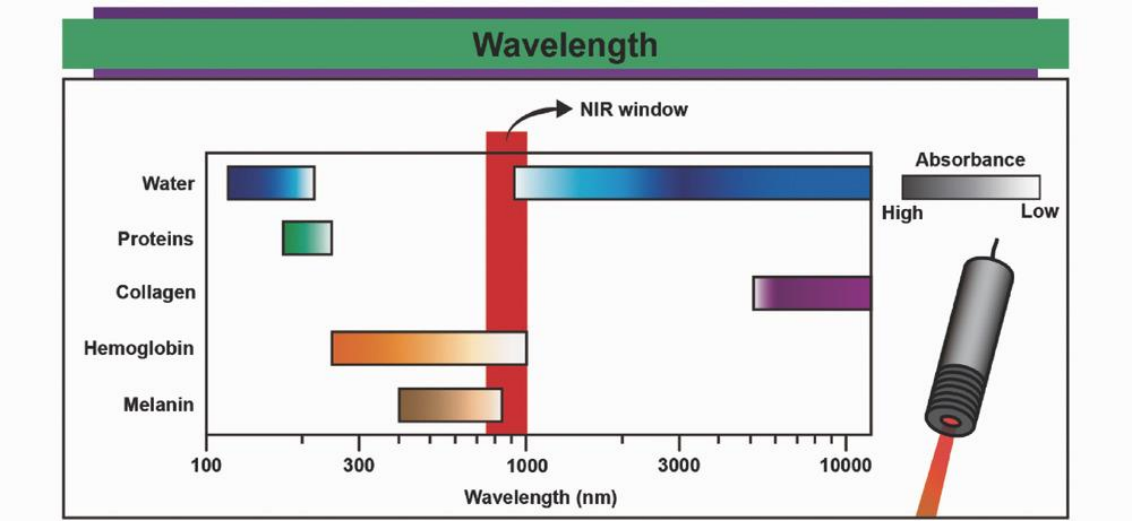

Figure 5: Schematic representation of the biological transparency window. The NIR light has a low interaction with the main constituents of the human body (water, proteins, collagen, hemoglobin and melanin), achieving a high penetration depth (Adapted from [17]).

Among these, GO has been widely explored for cancer PTT due to its NIR absorption [31, 32]. Furthermore, the aromatic lattice of GO can encapsulate a wide variety of therapeutics, enabling its use in NIR-responsive drug delivery applications [20, 33].

1.2 Graphene oxide in cancer photothermal therapy

1.2.1. Graphene oxide

GO is a 2D nanomaterial composed of a graphitic lattice functionalized with several types of oxygen-functional groups (hydroxyl, epoxide and carboxylic groups) [33-35]. To synthesize this nanomaterial, the most commonly used approaches (*e.g.* the Hummer's method, the Tour's method) involve the oxidation and chemical exfoliation of graphite, yielding graphite oxide [29, 36]. Then, graphite oxide is subjected to mechanical exfoliation (sonication, ultrasonication) yielding GO with nanometric dimensions (Figure 6) [34].

GO displays absorbance in the NIR region, and consequently can produce a temperature increase when irradiated with NIR light [29, 37]. In addition, the aromatic lattice of GO enables the encapsulation of chemotherapeutic drugs or other small molecules in its structure by hydrophobic interactions and/or π-π stacking [20, 38]. Furthermore, the oxygen-functional groups of GO endow it with adequate water solubility [29, 32, 33].

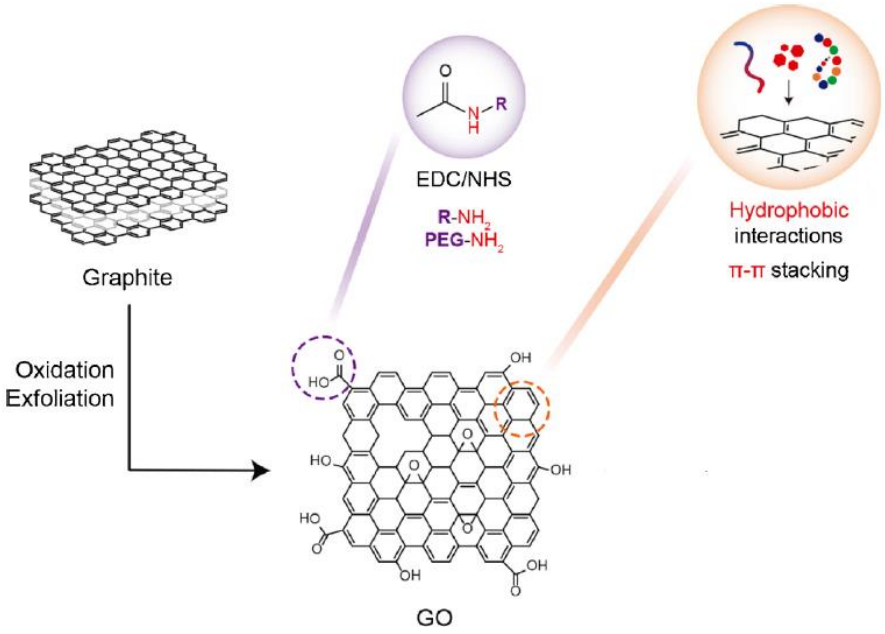

Figure 6: Schematic representation of the synthesis of GO and its functionalization using covalent and non-covalent interactions (Adapted from [29]).

Despite its potential, the direct application of as-synthesized GO in cancer photothermal therapy is hindered by its poor colloidal stability [20, 39]. As-synthesized GO precipitates in biological fluids and proteins rapidly become adsorbed on its surface, hindering its ability to reach the tumor site [20, 33, 40]. Furthermore, the interaction of GO with NIR light generates a modest photoinduced heat [41]. Therefore, it is necessary to administer high dosages of GO or to use intense radiation in order to exert an appropriate therapeutic effect [42-44]. In this way, addressing the GO poor colloidal stability and its suboptimal photothermal capacity is necessary to explore this nanomaterial for cancer PTT.

1.2.2. Strategies to improve GO colloidal stability

To increase the colloidal stability of GO, this nanomaterial has been functionalized with hydrophilic non-fouling materials [29, 45]. In this regard, GO can be functionalized by establishing covalent bonds between the carboxyl-groups of this nanomaterial and the primary amine-groups of polymers (Figure 6) [29, 37, 45]. On the other hand, the

aromatic lattice of GO can also be non-covalently functionalized using amphiphilic polymers through hydrophobic-interactions and/or π-π stacking (Figure 6) [29, 32].

In this context, Poly(ethylene glycol) (PEG) has been extensively used to functionalize GO derivatives aiming to improve their colloidal stability [46, 47]. For instance, de Melo-Diogo *et al.* verified that GO functionalized with D-*α*-tocopheryl polyethylene glycol 1000 succinate remained stable in water and culture medium supplemented with serum for up to 5 days [20]. Furthermore, Li *et al.* demonstrated that GO functionalized with PEG remained stable in water, phosphate buffered saline and cell culture medium supplemented with 10 % of Fetal Bovine Serum (FBS), even after 7 days of incubation [47].

Furthermore, the PEGylation of GO derivatives also increases their blood circulation time, leading to a higher tumor uptake [29]. Yang *et al.* showed that GO conjugated with PEG has a blood circulation half-life of ≈ 1.5 h, reaching a high tumor uptake in mice after 24 h [42]. In another study, Su *et al.* demonstrated that the doxorubicin blood half-life, when encapsulated in PEGylated GO, was 1.12 h, leading to a maximum tumor accumulation at 24 h post-injection [48].

However, there is an increasing body of information demonstrating that PEGylated nanomaterials can be immunogenic [49, 50]. Several authors have shown that anti-PEG antibodies are formed at the time of the first intravenous administration of PEGylated nanomaterials [51]. In subsequent administrations, these anti-PEG antibodies mediate the rapid clearance of the PEGylated nanostructures, hindering their tumor homing capacity - known as the Accelerated Blood Clearance (ABC) phenomenon [52]. In this regard, PEGylated GO derivatives have also been reported to suffer from the ABC phenomenon [53, 54]. Besides PEG, other materials such as bovine serum albumin and Dextran have been used to functionalize GO. However, GO derivatives functionalized with these materials present a tumor uptake inferior to that of PEGylated GO [29].

In this way, there is an urgent need to develop novel coatings to functionalize GO with the intent to improve its colloidal stability and blood circulation time, thus increasing the nanomaterial's likelihood to achieve tumor uptake through the static pores and dynamic vents occurring on the tumor vasculature [17, 19]. In this context, the functionalization of nanomaterials with zwitterionic brushes appears to be a promising approach [55, 56]. In particular, the modification of nanomaterials' surface with 2-(methacryloyloxy)ethyl]dimethyl-(3-sulfopropyl)ammonium hydroxide (SBMA) brushes has improved the nanostructures' resistance to protein adsorption and stability

in biological fluids [55, 57, 58]. Due to these properties, these nanomaterials can achieve a high tumor uptake [56, 57]. For instance, Peng *et al.* demonstrated that nanoparticles coated with SBMA present a 11-fold higher tumor accumulation than their non-coated equivalents [56]. Furthermore, SBMA-modified nanomaterials present a good biocompatibility and hemocompatibility [59, 60]. As importantly, SBMA coated nanostructures have not been reported to suffer from the ABC phenomenon [58, 61]. Despite these promising properties, GO derivatives functionalized with SBMA brushes have only be developed for use in membranes aimed for wastewater decontamination and hydrogels for cartilage replacement [62, 63]. In this way, the assembly of SBMA functionalized GO nanomaterials for application in cancer therapy should be pursued.

1.2.3. Strategies to improve GO heat conversion

Different strategies have been applied to increase the photothermal capacity of GO, and hence improve its phototherapeutic effect [29, 37, 64]. So far, the chemical reduction of GO has been the most explored approach [31, 65]. For such, GO is generally reduced using hydrazine hydrate [29, 66]. In this reduction process, the graphitic lattice of GO is restored, leading to an increase in the nanomaterials' NIR absorption and hence an enhancement of its photothermal capacity [66]. For instance, Yang *et al.* demonstrated that hydrazine hydrate reduced GO-based materials can exhibit 3-4 times greater NIR absorption than GO, thus producing a 14 °C greater photoinduced effect [46]. However, the reduced GO attained using hydrazine hydrate has a poor biocompatibility due to the high toxicity of this reducing agent [67].

Another strategy to improve the photoinduced heat generated by GO involves the incorporation of other NIR-responsive photothermal agents (*e.g.* gold nanorods, CuS nanoparticles, upconversion nanoparticles, Fe_3O_4 nanoparticles) on the surface of GO [68-71]. For example, aptamer-gold-GO nanohybrids can produce a 2.32-times higher temperature variation upon irradiation (808 nm, 3 W cm^{-2}, 5 min; 1.74 μg mL^{-1}) than GO (15.6 °C *vs.* 6.7 °C) [69]. However, the production of these hybrid nanomaterials is a process that is both laborious and complex, limiting their future translation.

Alternatively, NIR-responsive small molecules can also be incorporated into the GO surface to improve its photothermal effect. For example, Guo *et al.* demonstrated that PEGylated GO incorporating cypate (16.5 and 5.0 μg mL^{-1} of GO and cypate, respectively) induced a temperature variation of 33 °C after 5 min of NIR laser irradiation (785 nm, 1.5 W cm^{-2}). In turn, non-cypate containing GO (16.5 μg mL^{-1}) only produced a temperature increase of 13 °C, under the same conditions [72]. In this way, the

incorporation of NIR small molecules in GO is a promising strategy to enhance its photothermal capacity.

1.2.4. Functionalization of GO with zwitterionic brushes and loading of NIR small molecules

In order to improve the therapeutic potential of GO, it is crucial to address its poor colloidal stability and modest photothermal capacity. In this regard, the functionalization of GO with zwitterionic brushes and the loading of NIR small molecules in its structure appears to be a promising approach.

SBMA brushes are capable of improving nanomaterials' stability and blood circulation time, and have not been reported to experience the ABC phenomenon [57, 58, 61]. In order to functionalize GO with SBMA, the preparation of an amphiphilic polymer containing these segments may be a convenient route. For this purpose, SBMA could be grafted into Poly(ethyleneimine) (PEI) through a Michael addition. Then, the resulting polymer may be conjugated to hydrolysed Poly(maleic anhydride-*alt*-1-octadecene) (PMAO), using the carbodiimide chemistry, leading to the synthesis of SBMA-PEI-PMAO. The incorporation of PMAO is fundamental since this polymer can efficiently adsorb at GO surface through hydrophobic interactions [31]. In turn, IR780 displays a good photothermal capacity upon NIR laser irradiation and can be easily loaded on the GO structure through hydrophobic interactions [60, 73, 74].

1.3. Aims

The aim of this Master dissertation workplan was to prepare GO functionalized with an SBMA-based amphiphilic polymer (to improve GO colloidal stability) containing IR780 (to improve GO photothermal capacity) for application in breast cancer phototherapy.

The specific aims of this MSc workplan are:

- Synthesis of an SBMA-based amphiphilic polymer;
- Formulation and characterization of the physico-chemical and optical properties of IR780 loaded SBMA-functionalized GO;
- Characterization of the colloidal stability of the produced nanomaterials;
- Evaluation of the photothermal capacity of the produced nanomaterials;
- Determination of the cytocompatibility of SBMA-functionalized GO;
- Evaluation of the PTT mediated by IR780 loaded SBMA-functionalized GO on breast cancer cells.

Chapter 2

Experimental Section

2. Experimental Section

2.1. Materials

Michigan Cancer Foundation-7 (MCF-7) cell line and Normal Human Dermal Fibroblast (NHDF) were obtained from ATCC (Middlesex, UK) and Promocell (Heidelberg, Germany), respectively. 3-(4,5-dimethylthiazol-2-yl)-5-(3-carboxymethoxyphenyl)-2-(4-sulfophenyl)-2H-tetrazolium (MTS) was bought from Promega (Madison, WI, USA). FBS was acquired from Biochrom AG (Berlin, Germany). 1-Ethyl-3-(3-dimethylaminopropyl)carbodiimide (EDC) was purchased from Merck (Darmstadt, Germany). Dimethyl Sulfoxide (DMSO) and methanol were acquired from Fisher Scientific (Oeiras, Portugal). Cell imaging plates were obtained from Ibidi GmbH (Munich, Germany). Cell culture plates and T-flasks were purchased from Thermo Fisher Scientific (Porto, Portugal). GO was obtained from NanoPoz (Umultowska Poznan, Wielkopolska). PEI, SBMA, Dulbecco's Modified Eagle's Medium-F12 (DMEM-F12), IR780 iodide, *N*-Hydroxysuccinimide (NHS), paraformaldehyde, PMAO (average Mn 30000-50000 Da) and trypsin were bought from Sigma-Aldrich (Sintra, Portugal). Calcein-AM, Hoechst 33342® and Propidium Iodide (PI) were obtained from Thermo Fisher Scientific (Porto, Portugal). Water used in all experiments was double deionized (0.22 μm filtered, 18.2 MΩ cm).

2.2 Methods

2.2.1. Synthesis and characterization of SBMA-PEI-PMAO

The synthesis of SBMA-PEI-PMAO (SPP) was a tri-step process. Initially, SBMA was covalently attached to PEI following the method described by Venault *et al.* with slight modifications [75]. In brief, SBMA (1.176 g) and PEI (0.5 g) dissolved in 5 mL of water were reacted under reflux for 6 h at 90 °C. Then, the solution was dialysed against water (500-1000 Da molecular weight cut-off membrane) for 2 days and freeze-dried (ScanVac CoolSafe, LaboGene ApS, Lynge, Denmark), yielding SBMA-PEI (SP).

Subsequently, the hydrolysis of PMAO maleic anhydride rings was performed as we have previously described [73]. Briefly, an aqueous solution (4 mL) containing PMAO (0.2 g) and NaOH (2 N) was stirred for 5 h at room temperature. Then, the solution's pH was adjusted to 7 using HCl, followed by dialysis against water for 1 day (14000 Da molecular weight cut-off membrane). The recovered solution was freeze-dried, yielding hydrolysed PMAO.

Finally, to produce SPP, SP was attached to the hydrolysed PMAO carboxyl groups using the carbodiimide chemistry [31]. First, hydrolysed PMAO (50 mg) was activated with

EDC (6 mg) and NHS (3 mg) in 25 mL of DMSO. Subsequently, 50 mg of SP in water (25 mL) was added to the above solution. After reacting for 6 h at room temperature, the solution was dialysed against water for 3 days (14000 Da molecular weight cut-off membrane) and freeze-dried, yielding SPP.

As a control, PEI-PMAO (PP) was also produced as described above using hydrolysed PMAO (50 mg), PEI (50 mg), EDC (6 mg) and NHS (3 mg).

The successful synthesis of hydrolysed PMAO, SP, SPP and PP was confirmed by Fourier Transform Infrared Spectroscopy (FTIR) using a Nicolet iS10 spectrometer (Thermo Scientific Inc., MA, USA) with a spectral width ranging from 4000 to 600 cm^{-1}.

2.2.2. Assembly of IR780 loaded SPP functionalized GO

The assembly of IR780 loaded SPP functionalized GO (IR780-SPP/GO) was performed using a simple sonication approach as we have previously described [20]. Initially, an aqueous solution containing GO (100 μg mL^{-1}; 1 mL) and SPP (500 μg) was sonicated for 60 min (Branson 5800, Branson Ultrasonics, CT, USA). Then, IR780 (5 μg; dissolved in methanol) was added to the SPP-GO solution, followed by 30 min of sonication. Afterwards, this solution was dialysed (500-1000 Da molecular weight cut-off membrane) against water for 90 min and centrifuged to remove non-loaded IR780 and/or any aggregates, yielding IR780-SPP/GO. To produce IR780 loaded PEI-PMAO coated GO (IR780-PP/GO), the methodology was the same as described above but using PP instead of SPP. Non-loaded SPP/GO and non-loaded PEI-PMAO coated GO (PP/GO) were produced as described above without the IR780 addition step.

2.2.3. Characterization of nanomaterials' physicochemical and photothermal properties

The size distribution (in water) and zeta potential (in DMEM-F12 medium supplemented with FBS) of SPP/GO and IR780-SPP/GO were determined on a Zetasizer Nano ZS (Malvern Instruments Ltd., Worcestershire, UK). Furthermore, the colloidal stability of SPP/GO, IR780-SPP/GO, PP/GO and IR780-PP/GO was also evaluated in water and cell culture medium (DMEM-F12 supplemented with 10 % (v/v) of FBS). Transmission Electron Microscopy (TEM) was also used to confirm the lateral dimensions of SPP/GO, by using an HT7700 microscope (Hitachi, Japan) operated at an accelerating voltage of 100 kV (samples were stained with phosphotungstic acid (2 % (w/v))).

To verify SPP/GO and IR780-SPP/GO ability to interact with NIR light, the samples' absorbance was evaluated by UV-Vis-NIR absorption spectroscopy (Evolution 201

spectrophotometer, Thermo Fisher Scientific Inc., Massachusetts, USA). In turn, the photothermal capacity of SPP/GO and IR780-SPP/GO was determined by measuring the temperature variations induced by these nanoformulations (at different GO concentrations) over a period of 8 min of NIR irradiation (808 nm, 1.7 W cm^{-2}) with a thermocouple thermometer [73]. Water was used as a control.

Finally, the content of IR780 in SPP/GO was determined by absorption spectroscopy. For such, IR780-SPP/GO was resuspended in a water/methanol solution (1:1 (v/v)) and the sample's absorbance at 808 and 890 nm were analysed. First, the concentration of GO in IR780-SPP/GO was determined by using a standard curve of GO at 890 nm (IR780 and SPP do not absorb at this wavelength). Then, the determined concentration of GO and a standard curve of GO at 808 nm were used to find the absorption of GO at this wavelength. Subsequently, the absorption of GO at 808 nm was subtracted to that of IR780-SPP/GO at 808 nm, yielding the absorption of IR780 at 808 nm (SPP does not absorb at this wavelength). Finally, the absorption of IR780 at 808 nm and a standard curve of IR780 at this wavelength were used to determine the IR780 concentration. Then, the encapsulation efficiency of IR780 was determined as described in [73].

2.2.4. Evaluation of the cytocompatibility of SPP/GO

The cytocompatibility of SPP/GO towards MCF-7 cells (breast cancer cell model) and NHDF (normal cell model) was characterized using the MTS method as previously described by our group [76]. Cells were cultured in DMEM-F12 medium supplemented with 10 % (v/v) FBS and 1 % (v/v) streptomycin/gentamicin in a humidified incubator (37 °C, 5 % CO_2). Briefly, cells were seeded at a density of 1×10^4 cells per well in 96-well plates. After 24 h, the medium was replaced by fresh culture medium containing different concentrations of SPP/GO (1-50 μg mL^{-1} of GO equivalents). After 24 and 48 h, the medium was removed and cells were incubated with 120 μL of fresh medium containing MTS (20 μL) for 4 h (37 °C, 5 % CO_2). Then, cells' viability was determined by analysing the samples' absorbance at 490 nm using a microplate reader (Bio-Rad xMark microplate spectrophotometer). Non treated cells were used as the negative control (K^-) while cells treated with ethanol 70 % were used as the positive control (K^+).

2.2.5. *In vitro* evaluation of the phototherapeutic effect mediated by SPP/GO and IR780-SPP/GO

The photothermal effect mediated by SPP/GO and IR780-SPP/GO was evaluated as previously described by us [32]. Briefly, MCF-7 cells were seeded at a density of $1x10^4$ cells per well in 96-well plates. After 24 h, the medium was removed, and the cells were incubated with fresh medium containing different concentrations of SPP/GO

(at 30 and 50 μg mL^{-1} of GO equivalents) or IR780-SPP/GO (at 30/1.44 and 50/2.40 μg mL^{-1} of GO/IR780 equivalents). After 4 h of incubation, cells were irradiated with NIR light (808 nm, 1.7 W cm^{-2}, 8 min). After 24 h of incubation, cells' viability was determined using the MTS method as described in section 2.2.4.

To visualize the different phototherapeutic effects, MCF-7 cells incubated with SPP/GO (at 50 μg mL^{-1} of GO equivalents) or IR780-SPP/GO (at 50/2.40 μg mL^{-1} of GO/IR780 equivalents) and exposed to NIR light (as described above), were stained with Calcein-AM/PI (according to the manufacture's protocol) and were imaged by Confocal Laser Scanning Microscopy (CLSM) using a Zeiss LSM 710 confocal microscope (Carl Zeiss AG, Oberkochen, Germany) [73]. To analyse the uptake of IR780-SPP/GO by MCF-7 cells, these were incubated during 4 h with this nanomaterial. Afterwards, CLSM images were acquired by taking advantage from the IR780 intrinsic fluorescence [73].

2.2.6. Statistical analysis

To compare multiple groups, one-way Analysis of Variance (ANOVA) was used with the Student-Newman-Keuls test. A value of p lower than 0.05 ($p < 0.05$) was considered statistically significant. Data analysis was performed in GraphPad Prism v6.0 (Trial version, GraphPad Software, CA, USA).

Chapter 3

Results and Discussion

3. Results and Discussion

In order to improve the colloidal stability of GO, this nanomaterial was functionalized with a SBMA-based amphiphilic polymer (SPP). Then, the SPP-functionalized GO was loaded with IR780 with the intent to improve its photothermal capacity - Figure 7.

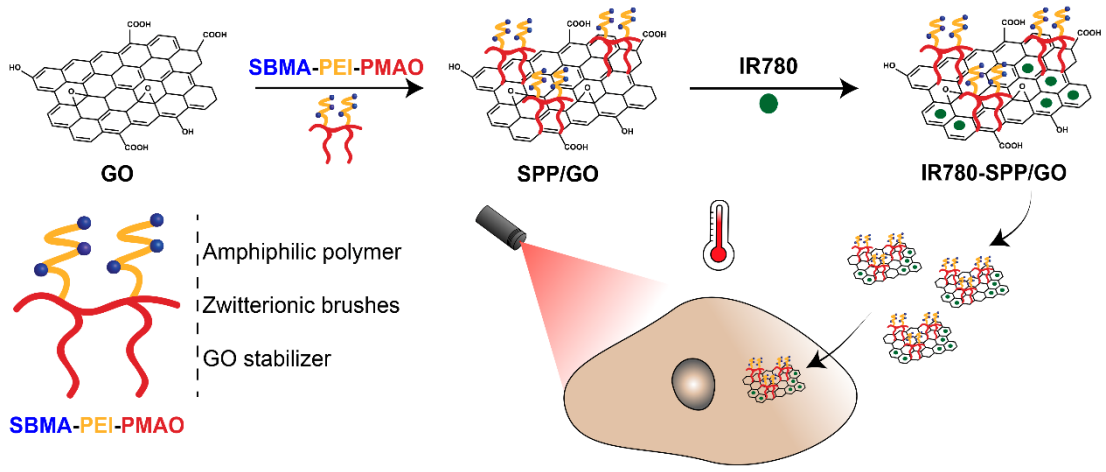

Figure 7: Schematic representation of SPP/GO and IR780-SPP/GO assembly and application in cancer therapy.

3.1. Synthesis and characterization of the SBMA-based amphiphilic polymer

The synthesis of the SBMA-based amphiphilic polymer (SPP) was achieved using a tri-step process. Initially, SBMA was grafted into PEI through a Michael addition. Then, the resulting polymer was conjugated to hydrolysed PMAO, using the carbodiimide chemistry, leading to the synthesis of SPP.

Then, the successfully synthesis of SPP was confirmed by FTIR (Figure 8 and 9). The spectrum of SBMA has a peak at 1035 cm^{-1} and 1165 cm^{-1} corresponding to the S=O stretch (Figure 8). In turn, the PEI spectrum displays peaks at 3347-3280 cm^{-1} (N-H stretch) and 1594 cm^{-1} (N-H bending) - Figure 8 [77, 78]. The spectrum of SBMA-PEI (SP) presents the SBMA and PEI characteristic peaks, hence confirming the grafting of SBMA into PEI (Figure 8).

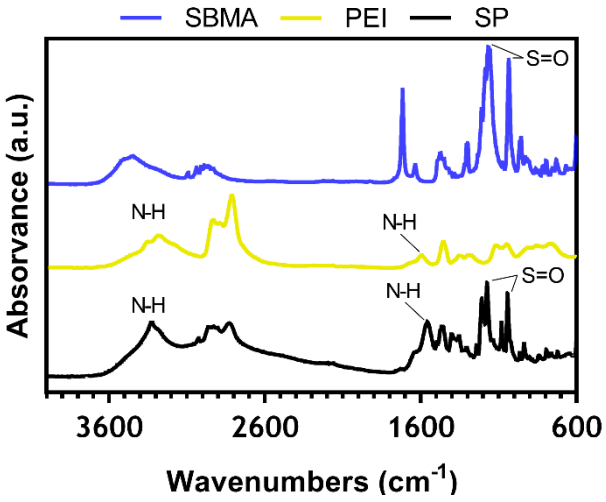

Figure 8: FTIR spectra of SBMA, PEI and SP.

The FTIR spectrum of hydrolysed PMAO displayed its characteristic peaks at 2920 cm^{-1} and 2851 cm^{-1} (C-H stretch) belonging mostly to its alkyl chain, as well as that at 1708 cm^{-1} (C=O stretch) corresponding to the hydrolysed PMAO maleic anhydride rings - (Figure 9) [31]. In turn, the FTIR spectrum of SPP presents the hydrolysed PMAO (C-H stretch) and SP (S=O stretch and N-H bending) signature peaks, hence confirming the conjugation of SP to hydrolysed PMAO (Figure 9).

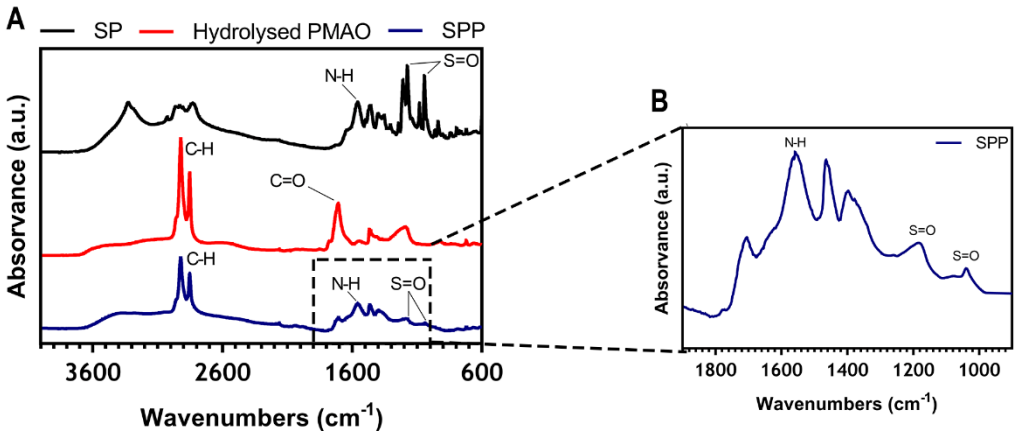

Figure 9: FTIR spectra of SP, hydrolysed PMAO and SPP (A). FTIR spectrum of SPP in the 1900-900 cm^{-1} wavenumber range (B).

As a control, the amphiphilic polymer without SBMA brushes was also prepared (PEI-PMAO (PP)), by covalently binding PEI to hydrolysed PMAO using the carbodiimide chemistry. The PP FTIR spectrum displayed the characteristic peaks of hydrolysed PMAO (C-H stretch) and of PEI (N-H bending), thereby proving its successful preparation (Figure 10).

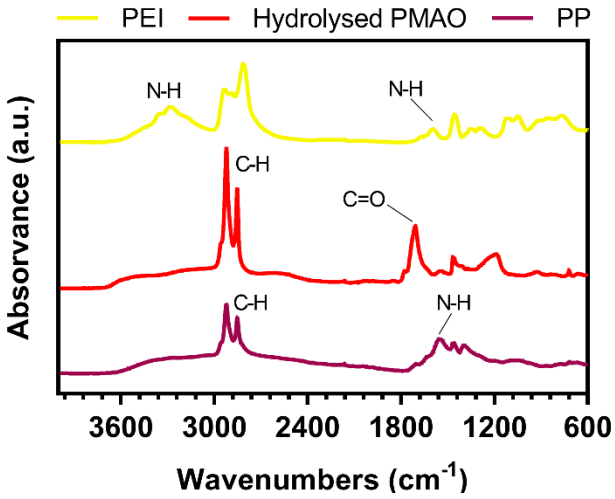

Figure 10: FTIR spectra of PEI, hydrolysed PMAO and PP.

3.2. Formulation and characterization of SPP/GO and IR780-SPP/GO

SPP was then used to functionalize GO through a simple sonication process, yielding SPP/GO. In this process, the alkyl chain of SPP adsorbs on the aromatic matrix of GO by taking advantage from hydrophobic-hydrophobic interactions. The Dynamic Light Scattering (DLS) analysis indicated that GO maintained its nanometric size distribution upon functionalization with SPP (Figure 11).

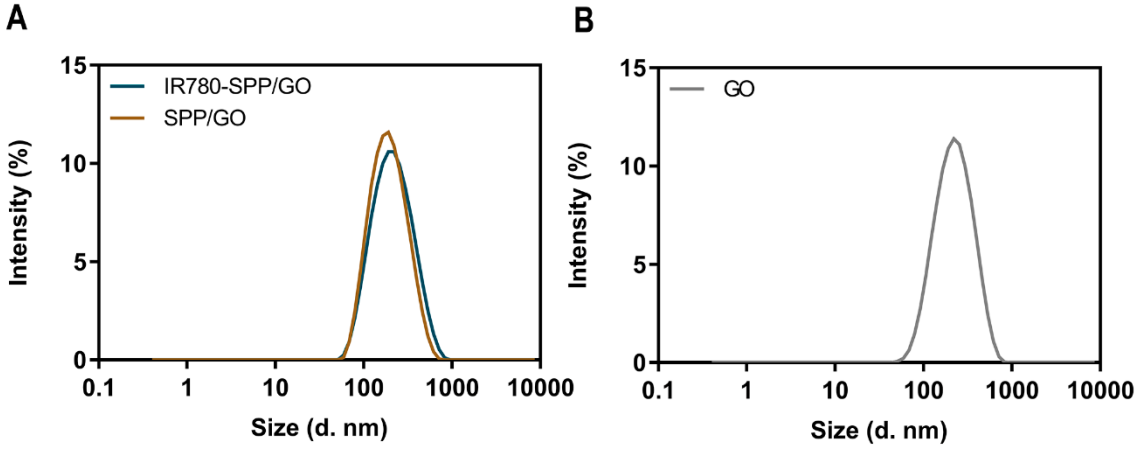

Figure 11: DLS size distribution of SPP/GO and IR780-SPP/GO (A) and GO (B).

The lateral dimensions of SPP/GO were then confirmed by TEM (Figure 12), revealing that this nanomaterial has a size compatible with its application in cancer therapy [17, 20].

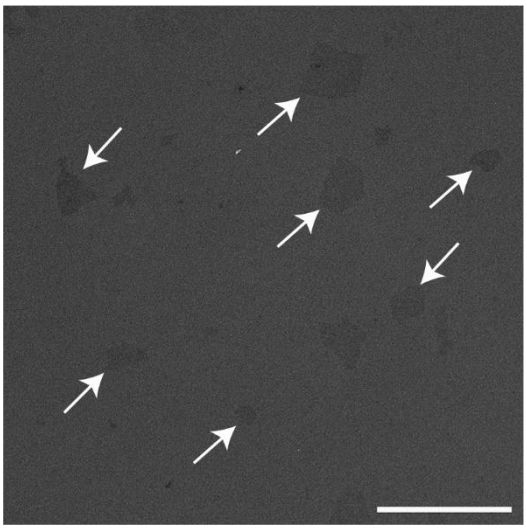

Figure 12: TEM image of SPP/GO. The white arrows indicate the SPP/GO nanosheets. Scale bar corresponds to 500 nm.

Then, IR780 was loaded on SPP/GO by taking advantage from hydrophobic interactions and π-π stacking. Both SPP/GO and IR780-SPP/GO demonstrated a similar size distribution, indicating that the IR780 loading does not affect the nanomaterials' size (Figure 11(A)).

The IR780 encapsulation efficiency in IR780-SPP/GO was of about 74 ± 1 %. Moreover, the water solubility of IR780 after being encapsulated in SPP/GO was 3.69 μg mL^{-1}. Considering that the water solubility of free IR780 is about 0.40 μg mL^{-1} [79], the IR780 loading into SPP/GO led to a 9.23-fold increase in its solubility. Furthermore, the IR780-SPP/GO adsorbed 0.048 ± 0.004 μg of IR780 per μg of GO, which is in line with the drug loading capacity of GO derivatives (please note that non-loaded GO is removed during the centrifugation step, leading to a higher drug loading capacity) [32].

The zeta potential of SPP/GO (- 7.7 ± 0.4 mV) and IR780-SPP/GO (- 8.1 ± 0.7 mV) revealed that these formulations are neutrally charged. Such is in agreement with the neutral charge displayed by several nanomaterials functionalized with SBMA brushes [57, 60, 80]. As importantly, neutrally charged nanomaterials (zeta potential between - 10 and + 10 mV) are considered in the literature as optimal due to their improved blood circulation time, which favours their tumor uptake [17].

Lastly, the colloidal stability of SPP/GO and IR780-SPP/GO overtime in water and in cell culture medium (DMEM-F12 supplemented with 10 % (v/v) of FBS) was assessed. Both SPP/GO and IR780-SPP/GO maintained their size distribution overtime (Figure 13 and 14(A)).

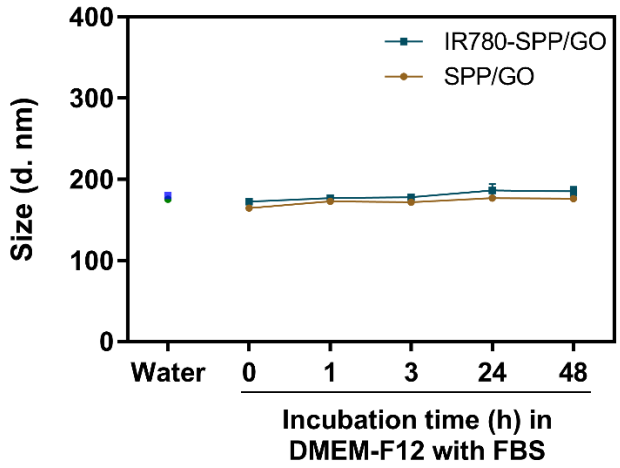

Figure 13: Size of SPP/GO and IR780-SPP/GO in water and in DMEM-F12 medium (supplemented with 10 % (v/v) of FBS) at different time points. Each bar represents the mean ± Standard Deviation (S.D.) (n=3).

As a control, the stability of PP/GO and IR780-PP/GO was also analysed, being verified that these non-SBMA grafted nanomaterials promptly precipitate in water and in culture medium (Figure 14(B)). In this way, the presence of the SBMA in the SPP/GO and IR780-SPP/GO grants these nanomaterials an excellent colloidal stability. In fact, the SBMA functionalization can reduce the adsorption of proteins on nanomaterials' surface, enhancing their stability during circulation as well as favouring their tumor uptake [57]. Together, this data indicates that the SPP/GO and IR780-SPP/GO have suitable physicochemical properties for application in cancer therapy.

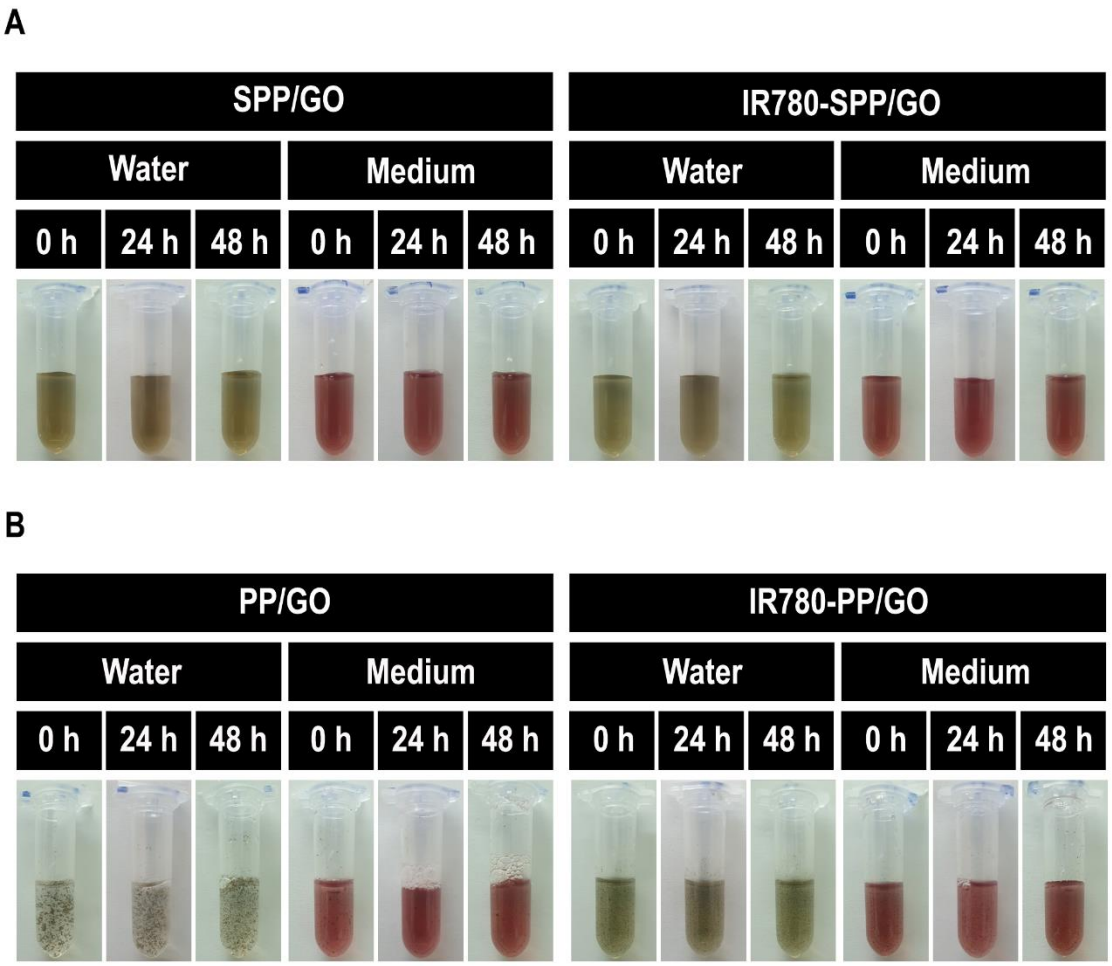

Figure 14: Macroscopic images of SPP/GO and IR780-SPP/GO in water and serum supplemented medium (DMEM-F12 supplemented with FBS (10 % (v/v))), at different time points (A). Macroscopic images of PP/GO and IR780-PP/GO in the same conditions (B).

3.3. Phototherapeutic capacity of SPP/GO and IR780-SPP/GO

To analyse the ability of SPP/GO and IR780-SPP/GO to interact with the NIR radiation, their absorption spectra was acquired (Figure 15(A)). As expected, SPP/GO demonstrated a broad absorption in the NIR region (750-1000 nm), which is a characteristic feature of GO derivatives [31, 32]. In turn, the absorption spectrum of IR780-SPP/GO (Figure 15(A)) displayed the GO characteristic absorption band as well as an increased absorption in the 680-870 nm range due to the presence of IR780 in this nanomaterial (Figure 15). Compared to SPP/GO, the IR780-SPP/GO presented a 2.7-fold higher absorption at 808 nm. Since 808 nm light will be used in the photothermal experiments, the enhanced absorption of IR780-SPP/GO at this wavelength may produce a better therapeutic outcome.

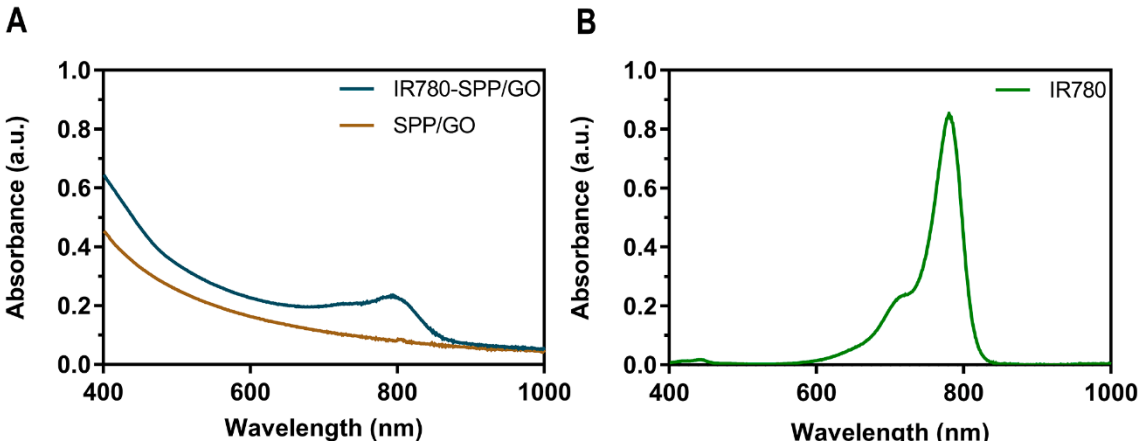

Figure 15: Optical properties of SPP/GO and IR780-SPP/GO. Absorption spectra of SPP/GO and IR780-SPP/GO (20 μg mL^{-1} of GO equivalents; in water) (A). Absorption spectrum of free IR780 (2.5 μg mL^{-1} of IR780; in methanol) (B).

Then, the photothermal capacity of SPP/GO and IR780-SPP/GO was investigated by exposing these nanomaterials to NIR light (808 nm, 1.7 W cm^{-2}, 8 min) and recording the temperature changes (Figure 16). At the maximum concentration tested (50 μg mL^{-1} of GO equivalents), the SPP/GO could produce a temperature increase to about 14.9 °C after 8 min of irradiation (Figure 16(A)). Such temperature variation is sufficiently high to cause damage to cancer cells [17, 22]. At the same concentration, the IR780-SPP/GO generated a temperature increase to 13.3 °C just after 2 min of irradiation (Figure 16(B)). After 8 min of laser exposure, the IR780-SPP/GO produced a photoinduced heat to 18.4 °C (Figure 16(B)). In this way, the incorporation of IR780 in GO derivatives can be pursued to improve their photothermal potential. Moreover, it was found that the NIR radiation does not increase meaningfully the water temperature (ΔT < 3.6 °C). Such result is explained by the minimal interactions of the NIR radiation with water, thus suggesting that SPP/GO and IR780-SPP/GO can produce a spatio-temporal controlled photothermal heating.

For instance, Ma *et al.* prepared gold clusters grafted into reduced GO (prepared using hydrazine hydrate) [81], that could generate a temperature increase of about 13.7 °C after 5 min of irradiation (808 nm, 2.2 W cm^{-2}) at a concentration of 90 μg mL^{-1} (of nanohybrids). Herein, the IR780-SPP/GO generated a photoinduced heat of 18.2 °C after 6 min of irradiation (808 nm, 1.7 W cm^{-2}) using only 50 μg mL^{-1} of GO. In this way, the incorporation of IR780 in GO is a promising alternative to using hydrazine hydrate for improving the GO photothermal capacity. Together, these results confirm the photothermal potential of IR780-SPP/GO.

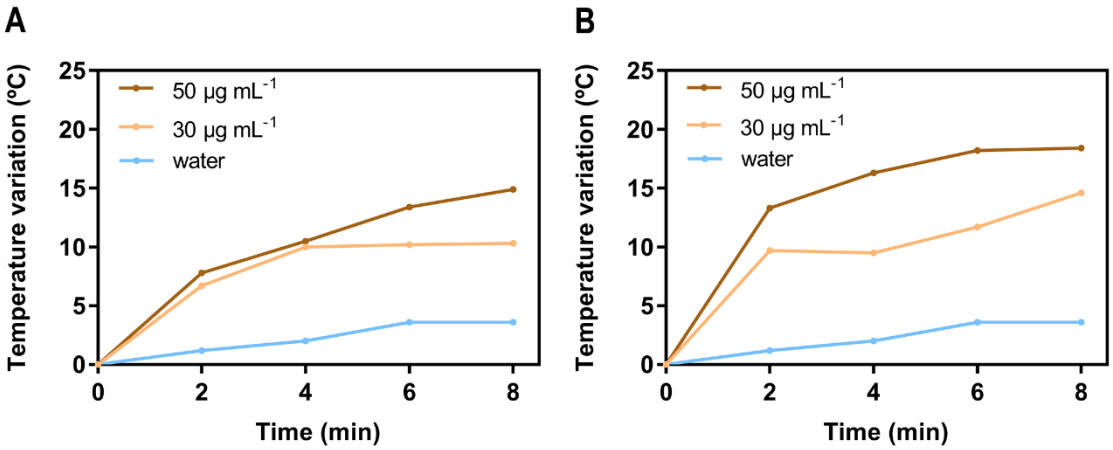

Figure 16: Photothermal properties of SPP/GO and IR780-SPP/GO. Temperature variation curves of SPP/GO (A) and of IR780-SPP/GO (B) at different concentrations (of GO equivalents) during 8 min of NIR irradiation (808 nm, 1.7 W cm^{-2}).

3.4. Cytocompatibility of SPP/GO

Before determining the phototherapeutic potential of SPP/GO, its cytocompatibility when non-irradiated with NIR light was determined (Figure 17). For such, MCF-7 cells and NHDF were used as models of breast cancer cells and healthy cells, respectively. Both MCF-7 cells (Figure 17(A)) and NHDF (Figure 17(B)) incubated with SPP/GO (up to 50 µg mL^{-1} of GO equivalents) did not suffer meaningful alterations on their viability, even after 24 and 48 h of incubation (cell viability > 86 %).

Several studies have reported that PEI incorporating nanomaterials can be cytotoxic due to the highly positive surface charge of this polymer [82-84]. For instance, Kievit *et al.* showed that PEI coated nanoparticles (zeta potential ≈ + 37 mV) are highly cytotoxic (cell viability was reduced to about 10 %) [82]. Herein, even though SPP contains PEI in its composition, the surface charge neutralization mediated by the SBMA grafting may have played a critical role in rendering SPP/GO cytocompatible. In fact, this data is also in line with the excellent biocompatibility of SBMA-functionalized nanomaterials [56, 60, 85].

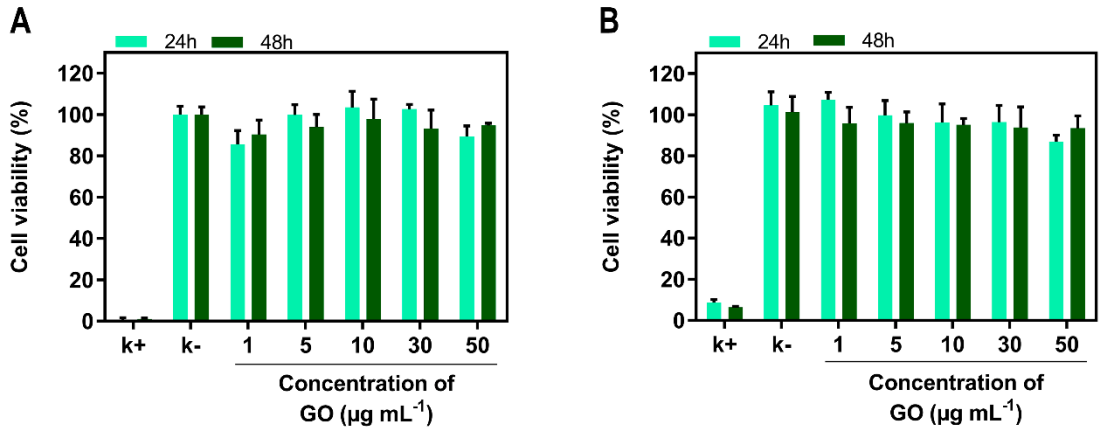

Figure 17: Evaluation of the cytocompatibility of SPP/GO. Cell viability displayed by MCF-7 cells (A) and NHDF (B) when incubated with SPP/GO, at different concentrations of GO, during 24 and 48 h. K^- represents the negative control and K^+ the positive control. Each bar represents the mean ± S.D. (n=5).

3.5. Phototherapeutic effect mediated by SPP/GO and IR780-SPP/GO

Finally, the phototherapeutic effect mediated by SPP/GO and IR780-SPP/GO towards MCF-7 cells was investigated (Figure 18(A)). As expected, non-irradiated SPP/GO and IR780-SPP/GO did not induce cytotoxicity towards MCF-7 cells (Figure 18(B)). Such is agreement with the cytocompatible profile of SPP/GO and with the fact that non-irradiated IR780-based nanomaterials are generally non-cytotoxic [60, 73, 86].

At the highest concentration tested (50 µg mL^{-1} of GO equivalents), the combination of SPP/GO with NIR light (808 nm, 1.7 W cm^{-2}, 8 min) only caused a reduction of breast cancer cells' viability to 73 % (Figure 18(B)). In stark contrast, the photothermal effect mediated by IR780-SPP/GO induced a reduction in the viability of cancer cells to about 20 % (Figure 18(B)). Therefore, by incorporating IR780 in the SPP/GO, its phototherapeutic capacity was increased by 3.65-times (Figure 18(B)). The enhanced therapeutic capacity of IR780-SPP/GO is related with its higher photothermal capacity when compared to that of SPP/GO (Figure 16). As importantly, MCF-7 cells treated with only NIR light did not suffer any meaningful alteration in their viability, which is in agreement with the weak/minimal interactions of this radiation with biological components.

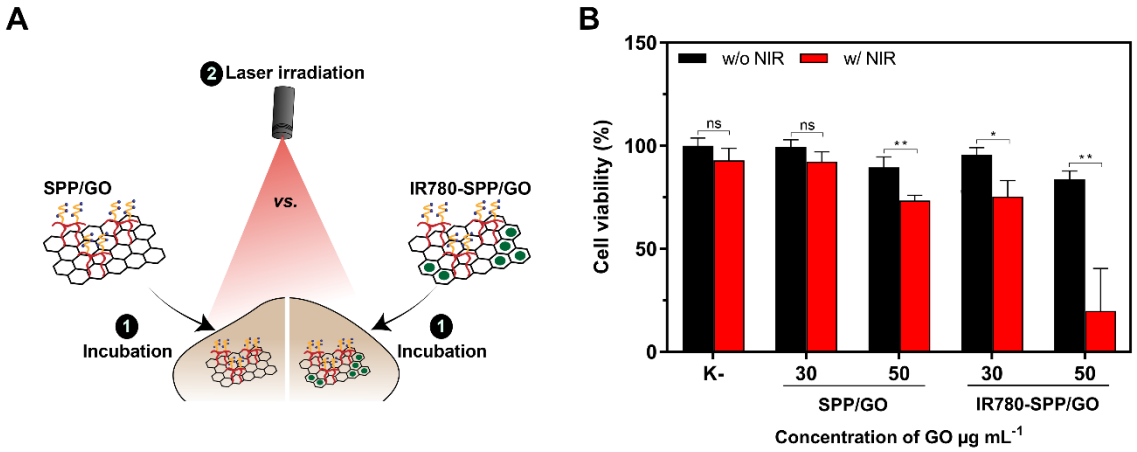

Figure 18: Determination of the therapeutic capacity of SPP/GO and IR780-SPP/GO. Schematic representation of the procedure used to evaluate the phototherapeutic effect of SPP/GO or IR780-SPP/GO towards MCF-7 cells (A). Therapeutic effect mediated by SPP/GO and IR780-SPP/GO towards MCF-7 cells without (w/o NIR) and with NIR (w/ NIR) laser irradiation (808 nm, 1.7 W cm^{-2}, 8 min) (B). K^- w/o NIR represents the negative control, while K^- w/ NIR represents cells solely treated with NIR light. Data represents mean ± S.D., n=5, (*$p < 0.01$, **$p < 0.0001$), ns = Non-significant.

To further confirm these results, the Calcein-AM (labels live cells) and PI (labels dead cells) staining of MCF-7 cells after the different treatments was performed (Figure 19). In agreement with the cell viability results, the CLSM images of cells exposed to SPP/GO, SPP/GO plus NIR light, and IR780-SPP/GO revealed that these were broadly stained with Calcein-AM (Figure 19). Accordingly, cells exposed to SPP/GO plus NIR light were stained with both Calcein-AM and PI (Figure 19(B)). Furthermore, a very high number of PI stained cells was imaged on the IR780-SPP/GO plus NIR light group (Figure 19(B)).

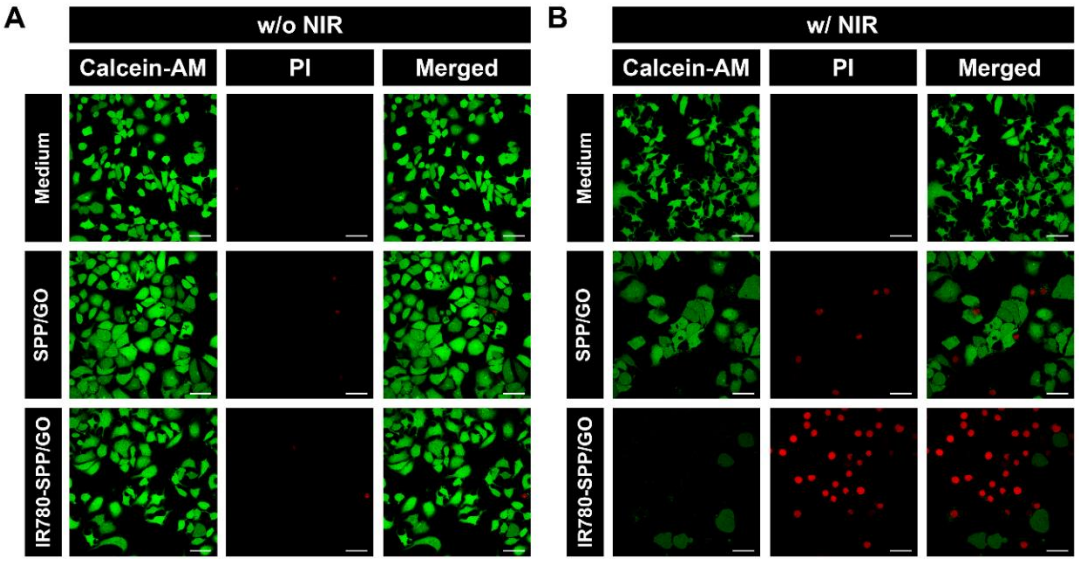

Figure 19: CLSM images of MCF-7 cells stained with Calcein-AM/PI after exposure to SPP/GO or IR780-SPP/GO w/o NIR (A) or w/NIR (B) laser irradiation (808 nm, 1.7 W cm^{-2}, 8 min). Medium w/o NIR represents the control for live cells, while medium w/ NIR represents cells solely exposed to NIR light. Green channel: Calcein-AM; Red channel: PI. Scale bars correspond to 50 μm.

The ability of IR780-SPP/GO to become internalized by MCF-7 cells was also confirmed by CLSM by taking advantage from the IR780 intrinsic fluorescence (Figure 20). Together, these results suggest that IR780-SPP/GO may produce an on-demand therapeutic effect upon NIR laser irradiation.

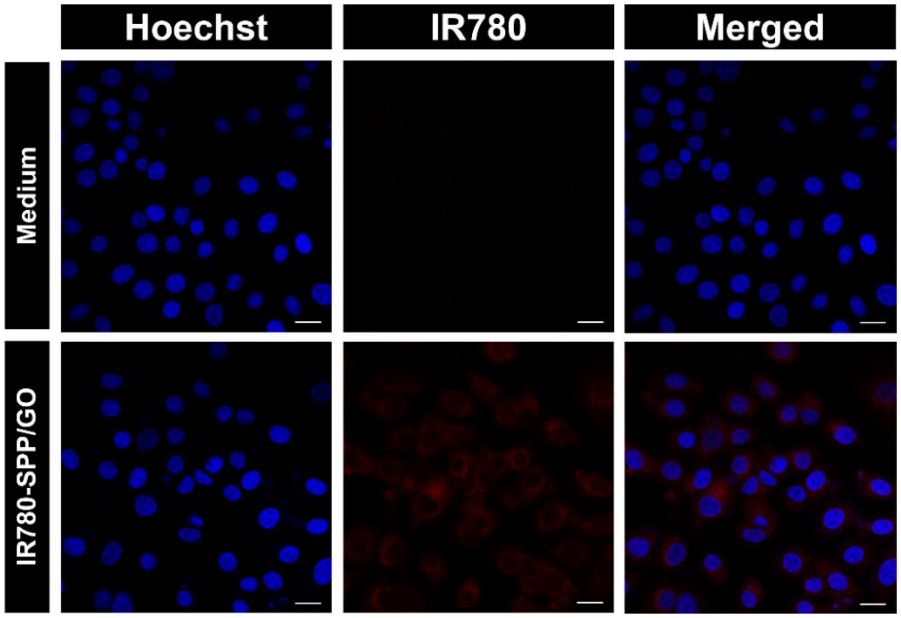

Figure 20: Cellular uptake of IR780-SPP/GO by MCF-7 cells. Cells solely incubated with medium were used as a control. Blue channel: Hoechst 33342® stained nucleus; Red channel: IR780. Scale bars correspond to 20 μm.

For instance, PEGylated polypyrrole-GO-gold nanohybrids, when administered at 60 μg mL^{-1}, could reduce the viability of cancer cells to 48 % upon NIR laser irradiation (808 nm, 1.75 W cm^{-2}, 10 min) [87]. In another work, the photothermal effect mediated by PEGylated GO/CuS hybrids induced a reduction of cancer cells' viability to 44 % at a concentration of 500 μg mL^{-1} of nanohybrids (980 nm, 1 W cm^{-2}, 10 min) [71]. In this study, the photothermal effect mediated by IR780-SPP/GO led to a decrease of cancer cells' viability to 20 %, using a low dose of photothermal agents (50/2.40 μg mL^{-1} of GO/IR780 equivalents) and a shorter irradiation time (808 nm, 1.7 W cm^{-2}, 8 min). In this way, IR780-SPP/GO are promising nanomaterials for the PTT of breast cancer cells.

Chapter 4

Conclusion and Future Perspectives

4. Conclusion and Future Perspectives

Despite all the intense research in the pursuit of novel breast cancer therapies, this disease remains one of the main causes of death among women. The high mortality of this disease can be attributed to the limitations of the clinically available breast cancer treatments (chemotherapy and radiotherapy), which display a low therapeutic efficacy (that is further aggravated by resistance mechanisms) and induce adverse side effects in patients.

To improve breast cancer treatment, researchers have recently started to explore new therapies (*e.g.* immunotherapy, phototherapy and gene therapy). Among them, the PTT mediated by nanomaterials has been displaying promising results. This type of approach explores the ability of NIR-absorbing nanomaterials with precisely-engineered physicochemical properties to become accumulated at the tumor site, and mediate upon NIR laser irradiation, a hyperthermia capable of causing the death of breast cancer cells.

Among the different nanomaterials that can be used for cancer PTT, GO has been receiving a great interest due to its NIR absorption and loading capacity. However, as-synthesized GO display a weak colloidal stability and subpar photothermal capacity. In this way, addressing these bottlenecks can lead to the development of GO based nanomaterials capable of mediating an improved breast cancer PTT.

During this last year, I performed the functionalization of GO with an amphiphilic polymer containing SBMA brushes and was loaded with IR780, for the first time, with the intent to improve its colloidal stability and phototherapeutic capacity. The results revealed that the SPP/GO and IR780-SPP/GO display a neutral surface charge and maintain their size distribution overtime when in contact with biological relevant media, demonstrating an improved colloidal stability. In contrast, the non-SBMA functionalized GO (PP/GO and IR780-PP/GO) promptly precipitated in this media. By loading IR780 into the SPP/GO, its NIR absorption increased by 2.7-fold, leading to a 1.2-times higher photothermal heating. In *in vitro* cell studies, the combination of SPP/GO with NIR light only reduced breast cancer cells' viability to 73 %. In stark contrast, by combining IR780-SPP/GO and NIR radiation, the cancer cells' viability decreased to 20 %. Overall, the IR780-SPP/GO presented an improved colloidal stability and enhanced photothermal capacity, rendering it a great potential for application in cancer PTT.

In the near future, the PTT mediated by IR780-SPP/GO towards 3D spheroids may be investigated. Due to the spheroids' ability to mimic the key features of the *in vivo* solid tumor (*e.g*. structural organization; physical and biochemical resistance patterns), this analysis will be crucial to further disclose the IR780-SPP/GO phototherapeutic potential. Moreover, the SPP amphiphilic polymer may be re-engineered in order to include targeting ligands (*e.g*. folic acid), which can improve the selectivity of the developed nanomaterials towards the breast cancer cells. Alternatively, drugs that have a higher cytotoxic effect on cancer cells than on healthy cells (*e.g*. D-*α*-Tocopherol succinate) may be incorporated on the IR780-SPP/GO to further enhance its selectivity.

Chapter 5

References

5. References

[1] I. Drake, J.A. Dias, S. Teleka, T. Stocks, M. Orho-Melander, Lifestyle and cancer incidence and mortality risk depending on family history of cancer in two prospective cohorts, International Journal of Cancer, 146 (2020) 1198-1207.

[2] R.L. Siegel, K.D. Miller, A. Jemal, Cancer statistics, 2020, CA: A Cancer Journal for Clinicians, 70 (2020) 7-30.

[3] Y.A. Fouad, C. Aanei, Revisiting the hallmarks of cancer, American Journal of Cancer Research, 7 (2017) 1016-1036.

[4] R. Brigelius-Flohe, A. Kipp, Glutathione peroxidases in different stages of carcinogenesis, Biochimica et Biophysica Acta (BBA)-General Subjects, 1790 (2009) 1555-1568.

[5] D. Hanahan, R.A. Weinberg, Hallmarks of cancer: the next generation, Cell, 144 (2011) 646-674.

[6] N.N. Pavlova, C.B. Thompson, The emerging hallmarks of cancer metabolism, Cell Metabolism, 23 (2016) 27-47.

[7] Y. Liu, T. Yin, Y. Feng, M.M. Cona, G. Huang, J. Liu, S. Song, Y. Jiang, Q. Xia, J.V. Swinnen, Mammalian models of chemically induced primary malignancies exploitable for imaging-based preclinical theragnostic research, Quantitative Imaging in Medicine and Surgery, 5 (2015) 708-729.

[8] B.C. Baguley, Multiple drug resistance mechanisms in cancer, Molecular Biotechnology, 46 (2010) 308-316.

[9] M.M. Gottesman, Mechanisms of cancer drug resistance, Annual Review of Medicine, 53 (2002) 615-627.

[10] F. Bray, J. Ferlay, I. Soerjomataram, R.L. Siegel, L.A. Torre, A. Jemal, Global cancer statistics 2018: GLOBOCAN estimates of incidence and mortality worldwide for 36 cancers in 185 countries, CA: a Cancer Journal for Clinicians, 68 (2018) 394-424.

[11] A.E. Place, S.J. Huh, K. Polyak, The microenvironment in breast cancer progression: biology and implications for treatment, Breast Cancer Research, 13 (2011) 227.

[12] K. Polyak, Breast cancer: origins and evolution, The Journal of Clinical Investigation, 117 (2007) 3155-3163.

[13] A.G. Waks, E.P. Winer, Breast cancer treatment: a review, Jama, 321 (2019) 288-300.

[14] C.E. DeSantis, J. Ma, M.M. Gaudet, L.A. Newman, K.D. Miller, A. Goding Sauer, A. Jemal, R.L. Siegel, Breast cancer statistics, 2019, CA: A Cancer Journal for Clinicians, 69 (2019) 438-451.

[15] M. Ewertz, A.B. Jensen, Late effects of breast cancer treatment and potentials for rehabilitation, Acta Oncologica, 50 (2011) 187-193.

[16] M.M. Leitão, D. de Melo-Diogo, C.G. Alves, R. Lima-Sousa, I.J. Correia, Prototypic heptamethine cyanine incorporating nanomaterials for cancer phototheragnostic, Advanced Healthcare Materials, 9 (2020) 1901665.

[17] D. de Melo-Diogo, C. Pais-Silva, D.R. Dias, A.F. Moreira, I.J. Correia, Strategies to improve cancer photothermal therapy mediated by nanomaterials, Advanced Healthcare Materials, 6 (2017) 1700073.

[18] J. Fang, H. Nakamura, H. Maeda, The EPR effect: unique features of tumor blood vessels for drug delivery, factors involved, and limitations and augmentation of the effect, Advanced Drug Delivery Reviews, 63 (2011) 136-151.

[19] Y. Matsumoto, J.W. Nichols, K. Toh, T. Nomoto, H. Cabral, Y. Miura, R.J. Christie, N. Yamada, T. Ogura, M.R. Kano, Vascular bursts enhance permeability of tumour blood vessels and improve nanoparticle delivery, Nature Nanotechnology, 11 (2016) 533-538.

[20] D. de Melo-Diogo, C. Pais-Silva, E.C. Costa, R.O. Louro, I.J. Correia, D-α-tocopheryl polyethylene glycol 1000 succinate functionalized nanographene oxide for cancer therapy, Nanomedicine, 12 (2017) 443-456.

[21] B. Liu, C. Li, Z. Cheng, Z. Hou, S. Huang, J. Lin, Functional nanomaterials for near-infrared-triggered cancer therapy, Biomaterials Science, 4 (2016) 890-909.

[22] K.F. Chu, D.E. Dupuy, Thermal ablation of tumours: biological mechanisms and advances in therapy, Nature Reviews Cancer, 14 (2014) 199-208.

[23] M. Chu, Y. Shao, J. Peng, X. Dai, H. Li, Q. Wu, D. Shi, Near-infrared laser light mediated cancer therapy by photothermal effect of Fe3O4 magnetic nanoparticles, Biomaterials, 34 (2013) 4078-4088.

[24] D. Jaque, L.M. Maestro, B. Del Rosal, P. Haro-Gonzalez, A. Benayas, J. Plaza, E.M. Rodriguez, J.G. Sole, Nanoparticles for photothermal therapies, Nanoscale, 6 (2014) 9494-9530.

[25] L. Cheng, C. Wang, L. Feng, K. Yang, Z. Liu, Functional nanomaterials for phototherapies of cancer, Chemical Reviews, 114 (2014) 10869-10939.

[26] E.S. Shibu, M. Hamada, N. Murase, V. Biju, Nanomaterials formulations for photothermal and photodynamic therapy of cancer, Journal of Photochemistry and Photobiology C: Photochemistry Reviews, 15 (2013) 53-72.

[27] C.F. Rodrigues, T.A. Jacinto, A.F. Moreira, E.C. Costa, S.P. Miguel, I.J. Correia, Functionalization of AuMSS nanorods towards more effective cancer therapies, Nano Research, 12 (2019) 719-732.

[28] N. Fernandes, C.F. Rodrigues, A.F. Moreira, I.J. Correia, Overview of the application of inorganic nanomaterials in cancer photothermal therapy, Biomaterials science, 8 (2020) 2990-3020.

[29] D. de Melo-Diogo, R. Lima-Sousa, C.G. Alves, E.C. Costa, R.O. Louro, I.J. Correia, Functionalization of graphene family nanomaterials for application in cancer therapy, Colloids and Surfaces B: Biointerfaces, 171 (2018) 260-275.

[30] Y. Dong, M. Gong, D. Huang, J. Gao, Q. Zhou, Shape memory, self-healing property, and NIR photothermal effect of epoxy resin coating with polydopamine@ polypyrrole nanoparticles, Progress in Organic Coatings, 136 (2019) 105232.

[31] R. Lima-Sousa, D. de Melo-Diogo, C.G. Alves, E.C. Costa, P. Ferreira, R.O. Louro, I.J. Correia, Hyaluronic acid functionalized green reduced graphene oxide for targeted cancer photothermal therapy, Carbohydrate Polymers, 200 (2018) 93-99.

[32] D. de Melo-Diogo, E.C. Costa, C.G. Alves, R. Lima-Sousa, P. Ferreira, R.O. Louro, I.J. Correia, POxylated graphene oxide nanomaterials for combination chemo-phototherapy of breast cancer cells, European Journal of Pharmaceutics and Biopharmaceutics, 131 (2018) 162-169.

[33] L. Yi, Y. Zhang, X. Shi, X. Du, X. Wang, A. Yu, G. Zhai, Recent progress of functionalised graphene oxide in cancer therapy, Journal of Drug Targeting, 27 (2019) 125-144.

[34] G. Gonçalves, M. Vila, M.T. Portolés, M. Vallet-Regi, J. Gracio, P.A.A. Marques, Nano-graphene oxide: a potential multifunctional platform for cancer therapy, Advanced Healthcare Materials, 2 (2013) 1072-1090.

[35] R.K. Singh, R. Kumar, D.P. Singh, Graphene oxide: strategies for synthesis, reduction and frontier applications, RSC Advances, 6 (2016) 64993-65011.

[36] D.C. Marcano, D.V. Kosynkin, J.M. Berlin, A. Sinitskii, Z. Sun, A. Slesarev, L.B. Alemany, W. Lu, J.M. Tour, Improved synthesis of graphene oxide, ACS Nano, 4 (2010) 4806-4814.

[37] D. de Melo-Diogo, R. Lima-Sousa, C.G. Alves, I.J. Correia, Graphene family nanomaterials for application in cancer combination photothermal therapy, Biomaterials Science, 7 (2019) 3534-3551.

[38] G. Chauhan, V. Chopra, A. Tyagi, G. Rath, R.K. Sharma, A.K. Goyal, "Gold nanoparticles composite-folic acid conjugated graphene oxide nanohybrids" for targeted chemo-thermal cancer ablation: in vitro screening and in vivo studies, European Journal of Pharmaceutical Sciences, 96 (2017) 351-361.

[39] Z. Liu, J.T. Robinson, X. Sun, H. Dai, PEGylated nanographene oxide for delivery of water-insoluble cancer drugs, Journal of the American Chemical Society, 130 (2008) 10876-10877.

[40] S. Wilhelm, A.J. Tavares, Q. Dai, S. Ohta, J. Audet, H.F. Dvorak, W.C. Chan, Analysis of nanoparticle delivery to tumours, Nature Reviews Materials, 1 (2016) 16014.

[41] D. Hu, J. Zhang, G. Gao, Z. Sheng, H. Cui, L. Cai, Indocyanine green-loaded polydopamine-reduced graphene oxide nanocomposites with amplifying photoacoustic and photothermal effects for cancer theranostics, Theranostics, 6 (2016) 1043–1052.

[42] K. Yang, S. Zhang, G. Zhang, X. Sun, S.-T. Lee, Z. Liu, Graphene in mice: ultrahigh in vivo tumor uptake and efficient photothermal therapy, Nano Letters, 10 (2010) 3318-3323.

[43] Y. Jin, J. Wang, H. Ke, S. Wang, Z. Dai, Graphene oxide modified PLA microcapsules containing gold nanoparticles for ultrasonic/CT bimodal imaging guided photothermal tumor therapy, Biomaterials, 34 (2013) 4794-4802.

[44] J.H. Lim, E.-J. Kim, C.D. Ahrberg, B.G. Chung, Functional graphene oxide-based nanosheets for photothermal therapy, Macromolecular Research, 26 (2018) 557-565.

[45] M. Alibolandi, M. Mohammadi, S.M. Taghdisi, M. Ramezani, K. Abnous, Fabrication of aptamer decorated dextran coated nano-graphene oxide for targeted drug delivery, Carbohydrate Polymers, 155 (2017) 218-229.

[46] K. Yang, J. Wan, S. Zhang, B. Tian, Y. Zhang, Z. Liu, The influence of surface chemistry and size of nanoscale graphene oxide on photothermal therapy of cancer using ultra-low laser power, Biomaterials, 33 (2012) 2206-2214.

[47] Y. Li, L. Feng, X. Shi, X. Wang, Y. Yang, K. Yang, T. Liu, G. Yang, Z. Liu, Surface coating-dependent cytotoxicity and degradation of graphene derivatives: Towards the design of non-toxic, degradable nano-graphene, Small, 10 (2014) 1544-1554.

[48] T. Su, F. Cheng, J. Yan, J. Cao, K. Luo, Y. Pu, B. He, Hierarchical nanocomposites of graphene oxide and PEGylated protoporphyrin as carriers to load doxorubicin hydrochloride for trimodal synergistic therapy, Journal of Materials Chemistry B, 6 (2018) 4687-4696.

[49] P. Zhang, F. Sun, S. Liu, S. Jiang, Anti-PEG antibodies in the clinic: Current issues and beyond PEGylation, Journal of Controlled Release, 244 (2016) 184-193.

[50] S.M. Fix, A.G. Nyankima, M.D. McSweeney, J.K. Tsuruta, S.K. Lai, P.A. Dayton, Accelerated clearance of ultrasound contrast agents containing polyethylene glycol is associated with the generation of anti-polyethylene glycol antibodies, Ultrasound in Medicine & Biology, 44 (2018) 1266-1280.

[51] T. Ishida, K. Atobe, X. Wang, H. Kiwada, Accelerated blood clearance of PEGylated liposomes upon repeated injections: effect of doxorubicin-encapsulation and high-dose first injection, Journal of Controlled Release, 115 (2006) 251-258.

[52] Y. Mima, Y. Hashimoto, T. Shimizu, H. Kiwada, T. Ishida, Anti-PEG IgM is a major contributor to the accelerated blood clearance of polyethylene glycol-conjugated protein, Molecular Pharmaceutics, 12 (2015) 2429-2435.

[53] N. Luo, J.K. Weber, S. Wang, B. Luan, H. Yue, X. Xi, J. Du, Z. Yang, W. Wei, R. Zhou, PEGylated graphene oxide elicits strong immunological responses despite surface passivation, Nature Communications, 8 (2017) 14537.

[54] H.-J. Im, C.G. England, L. Feng, S.A. Graves, R. Hernandez, R.J. Nickles, Z. Liu, D.S. Lee, S.Y. Cho, W. Cai, Accelerated blood clearance phenomenon reduces the passive targeting of PEGylated nanoparticles in peripheral arterial disease, ACS Applied Materials & Interfaces, 8 (2016) 17955-17963.

[55] S. Hua, J. Yu, J. Shang, H. Zhang, J. Du, Y. Zhang, F. Chen, Y. Zhou, F. Liu, Effective tumor-targeted delivery of etoposide using chitosan nanoparticles conjugated with folic acid and sulfobetaine methacrylate, RSC Advances, 6 (2016) 91192-91200.

[56] S. Peng, B. Ouyang, Y. Men, Y. Du, Y. Cao, R. Xie, Z. Pang, S. Shen, W. Yang, Biodegradable zwitterionic polymer membrane coating endowing nanoparticles with ultra-long circulation and enhanced tumor photothermal therapy, Biomaterials, 231 (2020) 119680.

[57] Y. Men, S. Peng, P. Yang, Q. Jiang, Y. Zhang, B. Shen, P. Dong, Z. Pang, W. Yang, Biodegradable zwitterionic nanogels with long circulation for antitumor drug delivery, ACS Applied Materials & Interfaces, 10 (2018) 23509-23521.

[58] J. Wu, W. Lin, Z. Wang, S. Chen, Y. Chang, Investigation of the hydration of nonfouling material poly (sulfobetaine methacrylate) by low-field nuclear magnetic resonance, Langmuir, 28 (2012) 7436-7441.

[59] Y.H. Huang, M.J. Wang, Atmospheric pressure plasma jet-assisted copolymerization of sulfobetaine methacrylate and acrylic acid, Plasma Processes and Polymers, 17 (2020) 1900209.

[60] C.G. Alves, D. de Melo-Diogo, R. Lima-Sousa, I.J. Correia, IR780 loaded sulfobetaine methacrylate-functionalized albumin nanoparticles aimed for enhanced breast cancer phototherapy, International Journal of Pharmaceutics, 582 (2020) 119346.

[61] S. Chen, L. Li, C. Zhao, J. Zheng, Surface hydration: Principles and applications toward low-fouling/nonfouling biomaterials, Polymer, 51 (2010) 5283-5293.

[62] G.S. Ibrahim, A.M. Isloor, A. Ismail, R. Farnood, One-step synthesis of zwitterionic graphene oxide nanohybrid: Application to polysulfone tight ultrafiltration hollow fiber membrane, Scientific Reports, 10 (2020) 6880.

[63] Z. Wang, J. Li, L. Jiang, S. Xiao, Y. Liu, J. Luo, Zwitterionic hydrogel incorporated graphene oxide nanosheets with improved strength and lubricity, Langmuir, 35 (2019) 11452-11462.

[64] A.F. Zedan, S. Moussa, J. Terner, G. Atkinson, M.S. El-Shall, Ultrasmall gold nanoparticles anchored to graphene and enhanced photothermal effects by laser irradiation of gold nanostructures in graphene oxide solutions, ACS Nano, 7 (2013) 627-636.

[65] C.K. Chua, M. Pumera, Chemical reduction of graphene oxide: a synthetic chemistry viewpoint, Chemical Society Reviews, 43 (2014) 291-312.

[66] P.-G. Ren, D.-X. Yan, X. Ji, T. Chen, Z.-M. Li, Temperature dependence of graphene oxide reduced by hydrazine hydrate, Nanotechnology, 22 (2010) 055705.

[67] J.T. Robinson, S.M. Tabakman, Y. Liang, H. Wang, H. Sanchez Casalongue, D. Vinh, H. Dai, Ultrasmall reduced graphene oxide with high near-infrared absorbance for photothermal therapy, Journal of the American Chemical Society, 133 (2011) 6825-6831.

[68] Y. Wang, H. Wang, D. Liu, S. Song, X. Wang, H. Zhang, Graphene oxide covalently grafted upconversion nanoparticles for combined NIR mediated imaging and photothermal/photodynamic cancer therapy, Biomaterials, 34 (2013) 7715-7724.

[69] L. Yang, Y.-T. Tseng, G. Suo, L. Chen, J. Yu, W.-J. Chiu, C.-C. Huang, C.-H. Lin, Photothermal therapeutic response of cancer cells to aptamer–gold nanoparticle-hybridized graphene oxide under NIR illumination, ACS Applied Materials & Interfaces, 7 (2015) 5097-5106.

[70] M.S. Khan, S. Pandey, M.L. Bhaisare, G. Gedda, A. Talib, H.-F. Wu, Graphene oxide@ gold nanorods for chemo-photothermal treatment and controlled release of doxorubicin in mice Tumor, Colloids and Surfaces B: Biointerfaces, 160 (2017) 543-552.

[71] J. Bai, Y. Liu, X. Jiang, Multifunctional PEG-GO/CuS nanocomposites for near-infrared chemo-photothermal therapy, Biomaterials, 35 (2014) 5805-5813.

[72] M. Guo, J. Huang, Y. Deng, H. Shen, Y. Ma, M. Zhang, A. Zhu, Y. Li, H. Hui, Y. Wang, pH-responsive cyanine-grafted graphene oxide for fluorescence resonance energy transfer-enhanced photothermal therapy, Advanced Functional Materials, 25 (2015) 59-67.

[73] C.G. Alves, D. de Melo-Diogo, R. Lima-Sousa, E.C. Costa, I.J. Correia, Hyaluronic acid functionalized nanoparticles loaded with IR780 and DOX for cancer chemo-photothermal therapy, European Journal of Pharmaceutics and Biopharmaceutics, 137 (2019) 86-94.

[74] C. Pais-Silva, D. de Melo-Diogo, I.J. Correia, IR780-loaded TPGS-TOS micelles for breast cancer photodynamic therapy, European Journal of Pharmaceutics and Biopharmaceutics, 113 (2017) 108-117.

[75] A. Venault, H.-S. Yang, Y.-C. Chiang, B.-S. Lee, R.-C. Ruaan, Y. Chang, Bacterial resistance control on mineral surfaces of hydroxyapatite and human teeth via surface charge-driven antifouling coatings, ACS Applied Materials & Interfaces, 6 (2014) 3201-3210.

[76] J.C. Boga, S.P. Miguel, D. de Melo-Diogo, A.G. Mendonça, R.O. Louro, I.J. Correia, In vitro characterization of 3D printed scaffolds aimed at bone tissue regeneration, Colloids and Surfaces B: Biointerfaces, 165 (2018) 207-218.

[77] Z. Luo, Q. Qi, L. Zhang, R. Zeng, L. Su, D. Tang, Branched polyethylenimine-modified upconversion nanohybrid-mediated photoelectrochemical immunoassay with synergistic effect of dual-purpose copper ions, Analytical Chemistry, 91 (2019) 4149-4156.

[78] X. Huang, H. Ishitobi, Y. Inouye, Formation of fluorescent platinum nanoclusters using hyper-branched polyethylenimine and their conjugation to antibodies for bio-imaging, RSC Advances, 6 (2016) 9709-9716.

[79] C. Jiang, H. Cheng, A. Yuan, X. Tang, J. Wu, Y. Hu, Hydrophobic IR780 encapsulated in biodegradable human serum albumin nanoparticles for photothermal and photodynamic therapy, Acta Biomaterialia, 14 (2015) 61-69.

[80] Z. Dong, J. Mao, M. Yang, D. Wang, S. Bo, X. Ji, Phase behavior of poly (sulfobetaine methacrylate)-grafted silica nanoparticles and their stability in protein solutions, Langmuir, 27 (2011) 15282-15291.

[81] W. Ma, Y. Hu, H. Yang, Y. Zhang, J. Ding, L. Chen, Au-aided reduced graphene oxide-based nanohybrids for photo-chemotherapy, Materials Science and Engineering: C, 95 (2019) 256-263.

[82] F.M. Kievit, O. Veiseh, N. Bhattarai, C. Fang, J.W. Gunn, D. Lee, R.G. Ellenbogen, J.M. Olson, M. Zhang, PEI–PEG–chitosan-copolymer-coated iron oxide nanoparticles for safe gene delivery: synthesis, complexation, and transfection, Advanced Functional Materials, 19 (2009) 2244-2251.

[83] S. Zhang, C. Kucharski, M.R. Doschak, W. Sebald, H. Uludağ, Polyethylenimine–PEG coated albumin nanoparticles for BMP-2 delivery, Biomaterials, 31 (2010) 952-963.

[84] S. Nimesh, A. Aggarwal, P. Kumar, Y. Singh, K. Gupta, R. Chandra, Influence of acyl chain length on transfection mediated by acylated PEI nanoparticles, International Journal of Pharmaceutics, 337 (2007) 265-274.

[85] A.G. Almutary, B.J. Sanderson, Z. Alhalili, A.V. Ellis, Toxicity of thiolated silica nanoparticles modified with sulfobetaine methacrylate for potential use in chemotherapy drug conjugation, Journal of Applied Pharmaceutical Science, 7 (2017) 001-009.

[86] J. Li, H. Hu, Z. Jiang, S. Chen, Y. Pan, Q. Guo, Q. Xing, Z. Jing, Y. Hu, L. Wang, Near-infrared-induced IR780-loaded PLGA nanoparticles for photothermal therapy to treat breast cancer metastasis in bones, RSC Advances, 9 (2019) 35976-35983.

[87] L. Xu, J. Wang, S.-Y. Lu, X. Wang, Y. Cao, M. Wang, F. Liu, Y. Kang, H. Liu, Construction of a polypyrrole-nased multifunctional nanocomposite for dual-modal imaging and enhanced synergistic phototherapy against cancer cells, Langmuir, 35 (2019) 9246-9254.